Environmental crises at the Permian–Triassic mass extinction

Jacopo Dal Corso[1]*, Haijun Song[1]*, Sara Callegaro[2], Daoliang Chu[1], Yadong Sun[3], Jason Hilton[4], Stephen E. Grasby[5], Michael M. Joachimski[3], Paul B. Wignall[6]*

[1]State Key Laboratory of Biogeology and Environmental Geology, School of Earth Science, China University of Geosciences, Wuhan, China.
[2]Centre for Earth Evolution and Dynamics, University of Oslo, Oslo, Norway.
[3]GeoZentrum Nordbayern, Friedrich-Alexander Universität Erlangen-Nürnberg (FAU), Erlangen, Germany.
[4]School of Geography, Earth and Environmental Sciences, University of Birmingham, Birmingham, UK.
[5]Geological Survey of Canada, Natural Resources Canada, Calgary, Alberta, Canada.
[6]School of Earth and Environment, University of Leeds, Leeds, UK.

*Correspondence should be addressed to J. Dal Corso (j.dalcorso@cug.edu.cn), Haijun Song (haijunsong@cug.edu.cn), and P.B. Wignall (P.B.Wignall@leeds.ac.uk).

Key points

- The Permian–Triassic mass extinction (252 Ma) resulted in a substantial reduction of global biodiversity, with the extinction of 81–94% of marine species and 70% of terrestrial vertebrate families.
- Sedimentary, palaeontological and geochemical records during the mass extinction indicate that a cascade of environmental changes caused the extinction.
- The environmental changes can be linked (and attributed to) the effects of volcanic emissions (for example CO_2, SO_2, and metals) during the eruption of the Siberian Traps large igneous province.
- Inferred volcanically driven environmental perturbations include global warming, oceanic anoxia, oceanic acidification, and (potentially) ozone reduction, acid rain, and metal poisoning.
- The crisis on land likely started ~60–370 kyrs before that in the ocean, indicating different response times of terrestrial and marine ecosystems to Siberian eruptions.

- The causes of marine extinctions are inferred from geochemical and sedimentary evidence, but the reasons for the earlier terrestrial ecological crises remain poorly understood, but likely include rapid atmospheric change.

Abstract

The link between the Permian–Triassic mass extinction (PTME; 252 Ma) and the emplacement of the Siberian Traps Large Igneous Province (STLIP) was first proposed over 30 years ago. However, the complex cascade of volcanic-driven environmental and biological events that led to the largest known extinction in life's history is still difficult to reconstruct. In this Review, we critically evaluate the geologic evidence and discuss the current hypotheses surrounding PTME kill mechanisms. Data indicate that the initial STLIP extrusive/pyroclastic volcanism was coeval with widspread crisis of terrestrial biota and marine animal species stress at high northern latitudes. The following onset of extensive magmatic intrusions is linked with the rapid (~60 kyr) extinction of 81–94% of marine species. The terrestrial to deep water extinctions are thought to have been caused by a combination of global environmental perturbations driven by the emissions from STLIP. Nevertheless, it remains difficult to understand the ultimate reason for the exceptional severity of the PTME. Future research needs improved geochronology of STLIP and sedimentary sequences (especially terrestrial) to better resolve the timing of volcanic phases and extinctions. Further ecological and physiological studies are needed to understand temporal and spatial extintion patterns. Improved modelling is necessary to reconstruct the causal relations between volcanism, environmental perturbations and ecosystem collapse.

Introduction

Many mass extinction [G] events punctuated the history of life and changed evolutionary trajectories [1]. Most of past biological crises are coeval with the emplacement of Large Igneous Provinces (LIPs) [G], which drove widespread environmental perturbations. LIP emissions of CO_2 and other gasses are comparable to current anthropogenic emissions, and future climate projections predict a scenario similar to the major Phanerozoic extinctions. Hence, undestanding past events will help define the tipping points that lead to a major biological crisis [2].

The Permian–Triassic mass extinction (PTME; 252 Ma) was the most severe biological crisis of the Phanerozoic (Fig. 1). It almost competely eliminated Palaeozoic fauna and flora, setting the stage for the evolution of modern ecosystems. Across the Permian–Triassic boundary (PTB), 81–94% of marine species went extinct [3–5] (Fig. 2 and 3). On land, 89% of tetrapod genera and 49% of families disappeared [6] (Fig. 4). Recovery began in the Early Triassic [7–9], but became significant only in the Middle Triassic, five million years later [10–12].

Data from the fossil, sedimentary, and geochemical record of the PTME suggest there were major environmental changes in marine and terrestrial settings [13–15] (Fig. 2 and 3). The global crisis is coeval with the emplacement of the Siberian Traps Large Igneous Province (STLIP) [16–18] (Fig. 5), that saw a relatively rapid (<1 Ma) eruption of 2–7 million km^3 [19–22] of basalt, together with volcanic emissions of CO_2, SO_2, halogens and metals that were capable of causing global climate and environmental catastrophe.

Detailed timing of events has improved remarkably in recent years thanks to advances in high-precision radioisotope dating [G], and high-resolution biostratigraphy [G] and chemostratigraphy [G] studies (especially C-isotope and Hg stratigraphy; BOX 1 and 2). Analysis of events from 252 million years ago at a high temporal resolution allowed identification of distinct phases of STLIP eruptions [18,23] and separate pulses of extinction among marine animals [4,24,25]. Particularly interesting developments include the increasing evidence that the terrestrial crisis was very likely underway several tens to hundreds of thousands of years before the marine extinction [26–28], clearly indicating that the PTME was not a single, instantaneous catastrophic event. Whilst these findings are expanding knowledge of STLIP volcanism, environmental changes, and extinction patterns, linking them remains difficult. The geological record tells a complex and partly obscure story of multiple, co-occurring phenomena, all playing a role in perturbing the ecosystems, and all probably interlinked in a cascade of environmental disasters.

In this Review we discuss the PTME pattern in the ocean and on land, the age and volcanic style of the STLIP, the evidence of a link between STLIP phases and the PTME, and the environmental crises triggered by the volcanic emissions and their role in the extinction and observed selectivity. We discuss the apparent diachrony between some recorded enviromental changes and extinctions. We then construct a likely chronology of the events based on the current evidence, propose a working hypothesis for future research, and highlight the open problems.

Pattern of the PTME

The exact temporal relationship between the marine and terrestrial extinctions is still debated. However, there is increasing evidence for an earlier onset of the terrestrial crisis and marine stress at high northern latitudes. The age and pattern of the marine PTME at low latitudes are very well constrained, and these provide a stratigraphic framework that allows the level of terrestrial crisis to be pinpointed. Here we examine the marine crisis first.

Marine extinction. Across the PTB, the Palaeozoic evolutionary fauna [G] was devastated at all ecological levels, resulting in the largest marine extinction of the entire Phanerozoic (Fig. 1a and Supplementary Information). It has been estimated that 81–94% of marine species went extinct [3–5].

The PTME appears to have been selective (Fig. 3). Some groups completely disappeared, such as trilobites, rugose and tabulate corals, fusulinid foraminifers, and blastoid echinoderms [4,29–31]; others, such as rhynchonelliforms (articulate brachiopods), crinoids, stenolaemate bryozoans, calcisponges, radiolarians, ammonoids, and ostracods, came close to annihilation with only a handful of surviving species [4,32]; whilst a few groups, including bivalves, gastropods, conodonts, and fishes, experienced "only" severe to moderate extinction rates [4,33–35] (Fig. 2). Extinction selectivity is not only evident in the taxonomic composition of the marine fauna, but also in ecological and physiological traits. Body-size selectivity is seen in foraminifers, conodonts brachiopods, and bivalves [36–39], with larger bodied organisms showing higher extinction rates, but this factor is less obvious in other groups [34,36,40] (Fig. 3).

It has been shown that physiologically buffered taxa that can regulate intracellular chemistry and counterbalance environmental chemical changes, like molluscs, ostracods, arthropods, and fish, experienced lower extinction rates than unbuffered taxa such as brachiopods and echinoderms [41–44] (Fig. 3). Moreover, non-motile taxa could in general be affected more by changing environmental conditions than motile animals, especially swimming animals [12]: Fish were relatively little affected compared to other groups [44]. However, statistical analysis shows that selectivity between these two groups was not significant (Fig. 3).

Taxa with limited geographic distribution are generally more prone to extinction than widely distributed groups because they are more dependent on local environmental conditions. However, this phenomenon is not so strong during the PTME [43,45,46] (Fig. 3), suggesting harsh marine environments were global in extent; there was no escape even for cosmopolitan species. Indeed, weak geographic range selectivity appears to be a general pattern with the major mass extinctions, being observed also at the end-Triassic and the end-Cretaceous [45] (Fig. 1a).

The pace of the PTME extinction pattern is long debated [32], with contrasting hypotheses of gradual *vs* abrupt extinction, and single *vs* discrete extinction pulses. The gradual disappearance of marine species observed in several PTB successions below the main extinction horizon [3,47] could be attributed, for most groups, to the Signor-Lipps effect [G] in the fossil record whereby rarer species are last recorded some time before their final demise [3,48,49]. The one exception is the ammonoid

extinction pattern observed in the succession of Iran where, considering the age confidence interval of each species, ammonoid diversity indeed shows a gradual decline before the PTME [47].

The marine extinction was a geologically brief event in the latest Permian–earliest Triassic [50]. Well-studied sections from South China, such as Meishan GSSP [G], show enormous losses at the base of the latest Permian *Clarkina meishanensis* zone [3,51]. Abrupt extinction in the latest Permian has also been documented in Italian foraminifera and Iranian brachiopods, foraminifera, and algae [48,52]. Thus, the crisis is often referred to as the end-Permian mass extinction, implying a single, geologically instantaneous (~30 kyr) event at the end of the Permian, just before the stratigraphic PTB [3,51] (Fig. 2). However, a significant diversity of Permian taxa, including brachiopods, foraminifers and ostracods survived beyond this level to become extinct either in the final part of the Permian or in the earliest Triassic [53–55]. Combining data from sections encompassing a spectrum of water depths shows that there was an especially intense final extinction phase in South China at the base of the *Isarcicella isarcica* Zone [4]. It is noteworthy that the second extinction pulse was proportionally intense but not as large in magnitude in terms of species loss.

Multi-phase extinction pattern has also been reported in the Dolomites, Italy [24,25]. Here, the main/first phase (which correlates to the first extinction pulse in South China), witnessed the loss of calcareous algae, foraminifera, and large-sized brachiopods and molluscs, with a genus extinction rate of 64% [25] (Fig. 2). 68% of survivors and newcomers subsequently went extinct in the interval ranging from the upper *H. changxingensis* to lower *H. parvus* zones [25], with a second extinction pulse that is somewhat slightly earlier than the second pulse in South China 4 (Fig. 2).

Adequate sampling obviously play an important role in the assessment of the extinction pattern. When fossil occurrences are rare, statistical confidence in the precise timing and number of pulses of extinction declines. Moreover, the importance of examining extinction patterns in different environments is highlighted by the record of foraminifer which shows a single extinction pulse in shallow platform facies but two episodes of extinction in deep slope facies [56]. In contrast, brachiopods suffered two episodic extinctions in shallow platform [57] and deep slope [3] and basin facies [58].

The latest U-Pb zircon ages from Meishan show that the two pulses of extinction happened at 251.941 and 251.880 Ma, respectively, separated by an interval of ~60 kyrs [59] (Fig. 2). It is unclear if the intervening interval should be considered a time of high stress or if the two pulses of extinction represent discrete events. The interlude was certainly an intriguing time, it saw the proliferation of microbialites and oolitic strata in low latitudes [60,61], whilst origination rates [G] increased [4], pointing

to a temporary improvement in environmental conditions either within the extinction interval, or between the two main extinction pulses (Fig. 2).

Terrestrial extinction. The PTME was the Phanerozoic's largest and most severe extinction of terrestrial plants and animals, at all latitudes and trophic levels (Fig. 4). Terrestrial floras suffered a worldwide catastrophic die-off of many plant groups in different geographical and climate zones during the PTME, which reset plant evolutionary history and was followed by an Early–Middle Triassic "coal gap": an interval in which peat-forming communities disappeared [10,26,62–67]. Some have argued that plant losses were much more moderate compared to animals [68,69], but the unprecedented abrupt shutdown of peat formation is a clear signal for major loss of terrestrial biomass across the PTB.

Plant fossil records from South China show that diversity and abundance of the tropical rainforest-type *Gigantopteris* flora experienced a sharp decrease with a loss of 95% of species and 50% of genera [70,71]. The Permian gymnosperm-dominated floras of North China and Russia experienced similar catastrophic losses at the same time [72]. In the southern hemisphere (Gondwana), the coal-forming *Glossopteris* flora went extinct (and coals disappeared) to be replaced by seed-fern shrubs (*Dicroidium*) [10,67,73], a stratigraphically long-ranging genus that survived the PTME and migrated polewards from low-latitudes [74]. The subsequent earliest Triassic floras throughout Eurasia and the southern continents were dominated by lycopods, especially *Pleuromeia*.

During the crisis, palynological data show widespread spore abundance spikes, accompanied by high abundances of spore tetrads and teratological [G] pollen, evidencing stressed conditions [67,75–83] (Fig. 4). Peak abundances of *Reduviasporonites* have been noted as marking fungal or algal bloom events. The former attribution would indicate proliferation of fungal saprotrophs during terrestrial ecosystem collapse [67,84–86], but the affinity of *Reduviasporonites* and its ecological significance remain controversial [87,88].

Major changes at the base of the terrestrial food-web, for example in the structure of floral communities from luxurious forests to less productive lycophyte-dominated floras, triggered a cascade of extinction in terrestrial ecosystems at all higher trophic levels [81,89]. It is therefore noteworthy, but perhaps not surprising, that the mass extinction was the only one to severely affect insects, with losses of 30% of orders and 50% of families [90–92].

Tetrapods were also severely impacted by the PTME with numerous families lost. Complex latest Permian ecosystems, dominated by herbivorous pareiasaurs, dicynodonts and carnivorous gorgonopsians, were replaced by ones with archosaurs and synapsids [93,94]. Global tetrapod generic

data suggest there was an 89% generic loss of tetrapods near the PTB [6]. Such losses within tetrapods could have happened during a "sustained extinction interval" of up to ~1 Myr, as seen in the fossil record from the Karoo Basin (South Africa) [95] (Fig. 4), although it is difficult to determine rates in the low quality tetrapod record. Many niches disappeared with studies showing the loss of all small fish- and insect-eaters, medium and large herbivores and large carnivores in Russia [94,96,97]. Coupled to the terrestrial extinction and vegetation loss, fluvial style changed across the PTME from meandering to braided rivers and aeolian systems, as observed in the successions of the Karoo Basin, Russia, Australia and North China (for example ref. [98]).

The timing of terrestrial ecosystem crisis relative to extinctions in the oceans is debated. Some studies argued that the terrestrial extinction was coeval with that in the oceans based on radioisotopic dating, chemostratigraphy and terrestrial information recorded in marine deposits [71,99,100]. However, recent high-resolution studies show that the terrestrial ecosystems were already stressed before the marine PTME (Fig. 4). Evidence of an earlier terrestrial crisis is based on improved stratigraphic frameworks including C-isotope stratigraphy (BOX 1), Hg (and Ni) spikes (BOX 2), magnetostratigraphy, and high-precision dating methods [26–28,95,101–103] that supersede previous lower resolution studies. This earlier crisis is seen in palaeofloras from the high-latitude Sydney Basin [26], in the tropical peatland ecosystems in equatorial South China [27], in the flora and fauna of North China [102], and in the tetrapod losses in the high-latitude Karoo Basin [28,95] (Fig. 4). Recurrent wildfire and abnormal pollen in the latest Permian also indicate that terrestrial ecosystems were under great stress before their collapse and prior to the subsequent marine extinction [26,27,78,101,102,104].

It is important to note that the terrestrial fossil record primarily derives from lowland settings, especially lacustrine and riparian environments where much sediment accumulates. This is especially the case for the plant record which is dominated by plants from wetlands, due to their good preservational conditions in such settings [105]. Much less is known about plants from drier and upland habitats which rarely fossilize, although evidence of upland vegetation loss during the PTME has been inferred from changing sedimentary facies in the Karoo Basin and Russia [106]. Wetland extinctions, that eliminated the *Glossopteris* and *Gigantopteris* mire communities, were not mirrored by equally severe losses in drier habitats dominated by conifers and pteridosperms [107,108]. This pattern may partly explain why the palynological record, which includes data of widely dispered pollen and spores from drier and upland habitats mixed with those of lowland floras, often shows a much more muted extinction intensity during the PTME [107,108].

The trigger

The two main agents suggested to be responsible for the environmental changes that led to the PTME—which will be discussed in the next section—are extraterrestrial impact or large-scale volcanism.

Extraterrestrial impact as the trigger of the PTME was proposed on the basis of geochemical (He^3 in fullerenes) and sedimentological (for example, the finding of chondritic meteorite fragments in the sedimentary record) data, and of the interpretation of a large structure found in the Indian ocean, the Bedout High, as a purporter impact crater of supposed PTME age [109,110]. However, the extraterrestrial impact hypothesis has been largely rejected bacause data have been proven to be difficult to reproduce, and the age and interpretation of the impact structure and geochemical changes have been questioned [111,112]. Most scientists now agree that there is negligible evidence to support extraterrestrial impact as the cause of the PTME.

In contrast, overwhelming data support that the PTME was triggered by the eruption of the STLIP. The STLIP was emplaced during the Permian–Triassic transition in the continental Tunguska Basin [18], the adjacent West Siberian Basin [113] and Taimyr Peninsula [21,114], with a poorly-constrained, original volume between 2 and 7 million km^3 [19,21,22] (Fig. 5). Changes in geochemistry and mode of emplacement of the STLIP magmas during its history, as seen in the most accessible lava pile sections (Norilsk, Putorana and Maymecha-Kotui) and in outcrops and boreholes from the Tunguska, Taimyr and West Siberian basins [18,115–119], reveal three phases of magmatic activity [23].

The oldest lava flows and pyroclastic [G] deposits were alkaline [G], mafic to ultramafic, and high in TiO_2 (>2 wt%) [117]. These magmas have a deep, pyroxenitic mantle source [G], and were rich in magmatic Cl [119–122]. The gases released by this high-volume, initial phase of magmatism were probably dominantly mantle-derived, products of recycled oceanic crust entrained by the mantle plume [119,122], although additional crustal sources are also likely [120,121,123]. This first phase of magmatism started just before 252.27±0.1 Ma, with extensive effusive activity taking place over the ~300 kyr preceding the marine PTME [18,23]. Intriguingly these early eruptions did not produce global changes in the $\delta^{13}C$ record nor in Hg concentrations (Fig. 5). However, northern latitude marine records downwind of the eruption site show pre-extinction shifts in the $\delta^{13}C$ and Hg records [124–126], suggesting limited atmospheric mixing of volatiles released in this early eruption phase. This first STLIP phase appears to have been coeval with widespread terrestrial crisis [26,27] (Fig. 5).

The second, tholeiitic [G] phase consisting of sills [G] and intrusions in the Tunguska Basin and Taimyr Peninsula began at 251.907±0.067 Ma, and is coeval with the onset of the marine PTME (Fig.

5). The apparent absence of effusive and/or explosive activity during this phase is debated and may reflect a lack of sampling in the region [114,127–131]. The tholeiitic phase magmas were derived from a shallow mantle pyroxenitic-peridotitic source [119,132], that underwent widespread interaction with the crust [132–136], and is poor in juvenile volatiles [G] [137]. During this subvolcanic phase the STLIP intruded a succession of coal, shales, sandstones, evaporites and carbonates in the Tunguska Basin [125,129,130] and their baking may have liberated a large amount of both greenhouse gases and halocarbons [123,129,130,132,138,139]. Explosive basalt pipes and breccia diatremes are widespread in the Tunguska Basin and are interpreted to have been the result of this gas generation and violent escape to the atmosphere [128,129,140,141] (although at least some may have erupted later in the Triassic [131]). Contact metamorphism of organic-carbon rich sediments around large-scaled sill intrusions in Taimyr and the Tunguska Basin (Siberia) likely produced large quantities of isotopically light CO_2 and CH_4 capable of changing the C-isotope signature of the atmosphere and ocean [21,125,129,138]. Indeed, the onset of intrusive magmatism, given analytical uncertainty, coincides with the start of the negative shift in $\delta^{13}C$ in the *C. yini* Zone (251.999 ±0.039 Ma; Fig. 2 and 5) [59], providing indirect support for this notion.

The third and last STLIP phase started at 251.483±0.088 Ma with renewed lava extrusion (alkaline), and ongoing intrusive activity (alkaline and tholeiitic), in the Maymecha-Kotui 118 and Taimyr regions [21]. These magmas are interpreted as extremely deep and hot products of a volatile-rich source [142], and were likely enriched in mantle-derived CO_2 [121]. A maximum age for the end of this phase, and STLIP activity overall, is placed at 250.2±0.3 Ma [18]. A gradual recovery of the $\delta^{13}C$ curve (BOX 1) towards pre-extinction levels is observed in the sedimentary record during the third phase (Fig. 5).

Environmental crises

The consequences of the volcanic emissions from the STLIP are considered in this section, including the emissions produced by contact metamorphism caused by magmatic intrusions in the host rocks, mainly CO_2 and CH_4, SO_2, halogens (for example, Cl, F, Br and halocarbons) and metals (for example, Hg, Cu). The multiple effects of these emissions are considered separately and are likely to have operated at different stages in the history of the PTME crisis (Fig. 6). Inferred environmental crises include global warming, oceanic anoxia, oceanic acidification, and (potentially) ozone reduction, acid rain, and metal poisoning.

Global warming. Among the gases released by volcanism, SO_2 has the potential to trigger short-term cooling episodes over a duration only a little longer than the eruptive interval [143,144]. This is too short

an interval to be detectable, given temporal resolution possible in deep time. Furthermore, it is a moot point whether such brief cooling intervals are capable of causing appreciable environmental stress, although episodic cooling events set in a context of longer-term warming could have damaged the ecosystems [144].

Instead, global warming, due to CO_2 and CH_4 emissions is the clearest signal to emerge from the eruption of LIPs. Temperatures across the PTB have been reconstructed using oxygen isotopes ($\delta^{18}O$) in conodont apatite and brachiopod calcite. Conodont $\delta^{18}O$ data from low latitude sections from Iran [145,146], Armenia [147] and South China [148–152], all indicate significant low-latitudinal warming of 8–10° C from the latest Permian to Early Triassic (Fig. 2 and 4). Despite differences between the analysed localities due to different palaeolatitude or depositional settings, calculated sea surface temperatures (SST) indicate pre-extinction (*C. nodosa*/*C. yini* Zone) SSTs of ~24–30°C that rapidly increased across the PTB and into the earliest Triassic SSTs (*C. isarcica* Zone), ultimately peaking at ~35–39°C [147]. Conodont $\delta^{18}O$ records indicate that temperatures increased over an interval of ~39 kyrs [147], although curiously the warming slightly postdates the initial shift in carbonate $\delta^{13}C$ [147,151] (Fig. 2).

Warming of 8–10° C likely resulted in a loss of performance of many marine organisms. High ambient temperatures increase metabolic activity and enhance oxygen demand, causing limited functional capacity of oxygen supply culminating in hypoxemia, anaerobic metabolism and loss of protein function [153]. Thermal tolerance of marine organisms is also linked with an organisms' level of metabolic activity, deoxygenation and also oceanic acidification [154,155]. Thus, warming may have been a major agent of the mass extinction. However, the first phase of the PTME occurred at the onset of warming when conditions may still have been relatively ameable (Fig. 2), and warming may have had a stronger role in the second extinction pulse in the earliest Triassic [4]. Lethally hot temperature may have induced selective extinction of marine animals and poleward migration [148,156,157].

However, two opposite patterns of selective extinction across latitudes had been reported [156,157] one showing the highest extinction rate in the high latitudes [157], the other documenting the highest rate in the tropics [156]. This discrepancy is likely due to the different statistical schemes used. Whilst higher polar extinction has been inferred, the study only considered the end-Permian extinction pulse [157] whilst higher tropical extinction is calculated considering two pulses (end-Permian and earliest Triassic) [156]. Likewise, in the marine fossil record of South China [4], the calculated extinction rate is 57% if only the first pulse is taken into account, and 93% including both pulses.

Poleward migration of about 10–15° is also observed in tetrapods [148,158]. In plants, elevated temperatures and droughts can inhibit photosynthesis, increase photooxidative stress due to higher

irradiance, burn leaves, and limit plants' growth and yield, and ultimately cause their death [159]. Warming could have also increased the prevalence of wildfire by increasing seasonality and drought (Fig. 3), for example as proposed for the records of South China where high charcoal abundance is found in strata recording the ~60 kyrs initial decline of $\delta^{13}C$, up to the onset of the marine crisis [27,104,160] (Fig. 2). Elevated fire activity would have aided post-fire run-off and erosion [104].

However, the terrestrial extinction appears to have started before the warming trend inferred from the $\delta^{18}O$ of conodont apatite (Fig. 2 and 4). In South China, declining $\delta^{13}C$ values coincide with high charcoal abundance [27] (Fig. 3) suggesting atmospheric pCO_2 was increasing during the interval of higher wildfire activity. Also, along the northwestern margin of Pangea marine environmental stress began prior to the main extinction event, suggesting that higher latitude oceans were deteriorating as the terrestrial extinction initiated [125,161,162]. Curiously, these changes occurred prior to the warming trend recorded by conodont $\delta^{18}O$ data.

Oceanic anoxia. The PTB coincides with a eustatic sea-level rise and the development of an oceanic anoxic event (OAE) [G] that has been directly implicated as a cause of the crisis [163]. However, marine anoxia during transgression is often encountered in the geological record, raising the question of why these conditions caused such a severe extinction crisis? There are likely to have been three reasons: the anoxia extended in some regions into extremely shallow waters [164], although oxic refugia remained [165]; the Panthalassa superocean also become anoxic throughout much of the water column [111,166]; the OAE persisted, with varying intensities, for several million years into the Middle Triassic, prolonging the stressful conditions for marine life [167–169]. Thus, both the extent and duration of anoxia were exceptional by Phanerozoic standards.

Evidence for anoxia is diverse and found in a broad range of environments. Organic-rich, pyritic, black shales, the typical manifestation of anoxic deposition, are best developed in the deep ocean sections now found in the accreted terranes in Japan and New Zealand [111,166,170]. Black shales are less common in shelf and epicontinental seaways, especially in tropical settings, perhaps due to high organic matter remineralization rates in hot sea water. In the low-latitude carbonate setting of Tethys, anoxic facies are usually developed as laminated, pyritic micrites such as in northern Italy [50]. In northern Boreal shelf seas, anoxic facies include finely-laminated, argillaceous strata and pyritic sandstones with abundant framboidal pyrite [G] [161,164].

Intensity of marine anoxia and its extent are inferred from geochemical data. The uranium isotope ratio of $^{238}U/^{235}U$ recorded in limestones shows a shift to lower values immediately prior to the first phase of mass extinction (Fig. 2): a change attributed to the accelerated removal of ^{238}U in anoxic

bottom waters [171]. The degree of anoxia driven metal drawdown was such that the oceans become depleted in trace metals [172]. The scale of anoxia also affected the ocean's sulphate budget. Increasingly heavy sulphate-sulphur isotope values in the Early Triassic, relates to removal of isotopically light pyrite sulphur, suggesting reduced seawater sulphate concentrations [173]. Biomarkers also provide evidence for oxygen-poor conditions including the presence of isorenieratane, an indicator that anoxic conditions extended into the photic zone [174].

The development of intensive anoxia profoundly altered the oceans' nutrient structure. Phosphorus recycling enhances under anoxic conditions [175] and, when combined with higher continental runoff, this leads to high phosphorus availability in the water column. However, nitrogen rather than phosphorus was more likely the limiting nutrient in the anoxic oceans of the time[176,177]. Thus, nitrogen isotope ratios show a significant decrease, from values up to ~10‰ to ~0%, in most of the basins across the PTB[177,178]. This suggests strong denitrification accompanied the onset of global anoxia, likely due to a fundamental shift from a nitrate-dominated to an ammonium-dominated nutrient supply which would normally favour nitrogen-fixing diazotrophs. However, diazotrophs require molybdenum and iron for nitrogen fixation and yet these are efficiently removed from anoxic waters, thereby causing a decrease in the ocean's total fixed-nitrogen and low levels of productivity [176]. Some alternative scenarios favour productivity increase during the extinction interval, driven by enhanced nutrient run-off [179], but these fail to account for the micronutrient limitations of diazotrophs in euxinic waters, as well as the absence of organic-rich shales in the Early Triassic [180].

The ultimate cause of the Permian–Triassic OAE has long been attributed to the effects of STLIP with warming and more sluggish ocean circulation usually invoked [111,163]. The Community Earth System Model with its embedded biogeochemical cycles, shows that an 11°C sea-surface temperature rise (a realistic value supported by $\delta^{18}O$ evidence [148]; Fig. 2 and 5), combined with increased freshwater runoff into high latitude seas, greatly increases ocean stratification and decreases meridional overturn circulation [157]. The result is a dramatic decrease in seafloor oxygenation. The model also successfully replicates regional variations with the best ventilated area shown to be the Perigondwanan margin of southern Tethys [157], a finding that closely matches field evidence from this region [54].

Oceanic acidification. Another potentially harmful effect of massive CO_2 injection into the atmosphere–ocean system is oceanic acidification (Fig. 6). Huge amounts of CO_2 entering the oceans acidifies water and decreases carbonate saturation. Evidence for oceanic acidification at the PTB comes from boron isotope ($\delta^{11}B$) and calcium isotope ($\delta^{44/40}Ca$) records [43,181,182] (Fig. 2), and the sediment record [43,162,183]. However, data from $\delta^{11}B$ of bulk carbonates, used to signify acidification during the second phase of the PTME during the *I. isarcica* Zone [184], are now generally considered

not to actually reflect marine pH [185]. Instead, a composite $\delta^{11}B$ record from pristine brachiopod shells from the Southern Alps (Italy) and South China shows a decline in $\delta^{11}B$ values, which suggests lowering of seawater *p*H, between the onset of the negative C-isotope excursion and the base of the *parvus* Zone, just above the PTB [182] (Fig. 2). This composite $\delta^{11}B$ record needs, however, further validation in other sections and improvement of temporal resolution. Ooidal limestones are widespread during the inferred lower pH interval [25], indicating saturated conditions, and the analysed brachiopods come from interbedded levels of microbialites [182]. The prevailing carbonates suggest that under saturation was not achieved. Acidification could have happened in very brief pulses, which are not recorded by low-resolution datasets, rather as a longer event between the onset of the marine extinction and the earliest Triassic [182].

A negative $\delta^{44/40}Ca$ shift during the PTME interval has been linked to the injection of CO_2 from the STLIP activity on the basis of its stratigraphic correlation with the negative $\delta^{13}C$ excursion [186]. Instead of solely indicating oceanic acidification, Ca-isotope data modelling suggests that a complex scenario controlled seawater $\delta^{44/40}Ca$ changes, involving CO_2 release, acidification, reduced skeletal carbonate sink, enhanced weathering of shelf carbonates, changes in carbonate mineralogy and changes in seawater saturation state [187,188]. In detail though, the negative $\delta^{13}C$ excursion (in bed 24 at Meishan) predates the negative $\delta^{44/40}Ca$ shift (which occurs above bed 25 [186]; Fig. 2), complicating the interpretation of the relationships between the Ca- and C-isotope records. Similar negative $\delta^{44/40}Ca$ excursions, recorded by both conodont apatite and bulk carbonate, are seen at the same stratigraphic interval in other localities [188–191].

More indirect evidence for oceanic acidification comes from the fossil record which shows that the crisis saw the preferential extinction of physiologically unbuffered taxa, with low metabolisms and high energy demand for the production of calcium carbonate skeletons (for example corals, brachiopods, calcareous sponges, and foraminifera), whilst well-buffered taxa (for example bivalves, gastropods, ammonoids and conodonts) could have survived the crisis relatively better [4,43,192].

Analysis of the microstructure of brachiopod shells provides evidence to suggest a role for acidification in brachiopod extinction losses. All brachiopod groups suffered severe losses with the diverse Strophomenata going extinct. The Rhynchonellata fared somewhat better and it has been suggested that their higher shell organic content enabled them to better survive acidified conditions [183]. However, at lower taxonomic order the Rhynchonellata suffered severe losses and their story during the PTME could also be described as a successful re-radiation of the survivors in the earliest Triassic that saw some genera become widespread [193]. In addition, the preferential extinction of coarsely

ornamented ammonoids supports the pressure of oceanic acidification on shell-building costs for shelled animals [194].

Along the north western margin of Pangea there is also a gradual loss of carbonate producers through the late Permian creating an empty ecologic niche that was filled by siliceous sponges expanding from deep environments to become the dominant organism in late Permian shallow shelfs [161,162], suggesting decreasing pH prior to the extinction.

Ozone disruption. High abundance of teratological sporomorphs during the PTME (Fig. 4) has been attributed to increased UV-B radiation due to disruption of the ozone layer [76,78,81,195]. Experiments on living *Pinus mugo* showed increasing exposure of plants to UV-B radiation induced malformation on pollen grains similar to those observed at the PTME and, although all trees survived, their fertility markedly decreased [81]. Therefore, higher UV-B radiation and lower plant fertility may have triggered a collapse of the whole terrestrial ecosystem by shutting down most primary productivity.

Ozone depletion could have been driven by the release of halogens and halocarbon compounds from volcanic activity and the combustion of coals and evaporites intruded by STLIP [196–198] (Fig. 5). However, the first explosive phase of STLIP activity appears to be coincident with the early terrestrial decline of plants and the first occurrences of teratological sporomorphs (Fig. 4), whilst the release of halocarbons (for example CH_3Cl) from contact metamorphism (intrusive phase) is thought to have the strongest impact on the ozone layer [197,198]. Teratological sporomorphs are found throughout the PTME (Fig. 4), but ozone is quickly (~10 yrs) restored in the atmosphere, hence making a long-term disruption of the global ozone unlikely [198].

Acid rain. Teratological sporomorphs (Fig. 4) alone are not a direct evidence of UV-B radiation, as they could be the result of other stresses such as acid rain [81,198] and metal poisoning [82]. Acid deposition can potentially kill plants, phytoplankton, vertebrates and invertebrates in terrestrial aquatic ecosystems, and acidification of non-calcareous soil results in leaching of important nutrients (Ca, Mg and K), with the effect of weakening plants and increasing their mortality rate [199].

Magmatic degassing of SO_2 and halogens from STLIP could have driven acid rain [198]. Earth system modelling shows that, alongside the previously discussed ozone damage, S injected into the stratosphere during STLIP pyroclastic activity (Fig. 5) could have triggered extensive acid rains at the PTB, although these were only severe (pH = 2) in the Northern Hemisphere [198].

Possible direct evidence of acid rain comes from one section in northern Italy, where the abundance of vanillin—a product of pH-dependent enzymatic decomposition of organic matter in soil—could

suggest pulses of soil acidification [200]. Vanillin peaks occur before the marine extinction interval (latest Permian) [25]. Hence, acid rains may have affected terrestrial ecosystems already before the onset of the marine extinction (Fig. 5). Significantly, PTB palaeosols in Antarctica show high chemical weathering but no indication of acid conditions; there was no leaching of Ca and Mg [201].

Other geochemical evidence for acid rain comes from sulfur isotope and concentration records in the Karoo Basin (South Africa), where higher accumulation of sulfide was interpreted as the effect of high sulfate supply to the freshwater environment from acid rain [202]. However, the terrestrial extinction in the Karoo Basin began before the S geochemical changes, making their significance moot. Currently, exept for these local datasets, there is no conclusive evidence that widespread acid rain triggered the terrestrial collapse in the latest Permian, especially not in the southern hemisphere.

Metal poisoning. Potentially, metal poisoning may have occurred in marine environments, where an increase of concentration of toxic metals (Hg, Cr, As, and Co) is observed [125,126,161]. High concentrations of Hg, the most toxic metal, may have been reached after the marine extinction, when the reduction of bioproductivity could have led to a decrease of Hg drawdown by organic matter and its potential build-up in marine environments to toxic levels, before it was removed by sulphide deposition [126].

A coincidence between a peak of teratological lycophyte spore tetrads [G] and high Hg and Cu concentrations has been found a short distance above the terrestrial extinction level in South China, indicating that the survivor plants might have experienced stress caused by higher metal concentrations in the environment [82] (Fig. 4). Reduced plant transpiration, changes to the hydrological cycle and climatic drying following terrestrial vegetation loss may have resulted in reduced water availability in freshwater ecosystems leading to such metal concentrations increase. Hg is generally thought to derive from volcanic activity [203], but Hg isotopes and modelling of Hg cycling indicate that, superimposed on a general increase of volcanic Hg deposition across the PTME, further Hg could have been released into the environment due to massive oxidation of terrestrial organic matter and soil following the collapse of land ecosystems [204] (BOX 2). Similar behaviour could have sourced Cu [82]. Hence, the increase of metal loading in South China during the PTME might actually be the consequence of the demise of the *Gigantopteris* rainforests and wetland species [204].

Linking kill mechanisms and extinction patterns

The latest high-resolution chronology of the PTME (Fig. 6) suggests that the terrestrial ecological disturbance could have started 60–370 kyr before the marine extinction [26–28,95,101–103]. This was coincidental with the initial, mostly explosive phase of STLIP. However, the temporal resolution of the terrestrial extinctions remains more poorly known than that of the marine extinctions and may have been spread over ~1 Myr [95].

The terrestrial extinction mechanism is not clear, and mainly inferred by indirect, often local, and mainly palaeontological proxies (Fig. 6). Increased seasonality during the initial stage of the negative $\delta^{13}C$ (Fig. 6) could have lead to increase of wildfires [27]. Declining $\delta^{13}C$ values coeval with higher charcoal abundance suggest addition of isotopically light CO_2 to the ocean–atmosphere system and that warming may have played a role. However, the available temperature proxy from marine settings (conodont $\delta^{18}O$) suggests temperatures did not begin to increase until after the terrestrial crisis had begun (Fig. 2 and 5).

Temporal decoupling of terrestrial extinctions predating marine extinctions is intriguing and suggests spatial heterogeneity in the extinction patterns and potentially mechanisms. Delayed onset of marine extinctions may be partially related to thermal inertia of the oceans and their higher thermal capacity compared to land that heats and cools quicker [205], but ocean turnover times occur in the order of 1000 years [206] so are unlikely to have operated at a 60–370 kyrs time scale.

Terrestrial stress may have come from emissions of SO_2 and halogens and their consequent acid rains [202], and disrupted ozone shield [76,81]. Increasing UV-B radiation on Earth's surface and acid depositions could have had lethal effects on terrestrial ecosystems, causing stress to the vegetation, lowering plants' fertility and eventually leading to their death, with repercussions at all higher trophic levels. However, long-term disruption of the global ozone during the PTME is unlikely [198].

It is not clear what was the effect on marine ecosystems of the first phase of the STLIP activity (Fig. 6). Beds of coal ash and associated Hg spikes are observed in northwest Pangea prior to the main negative $\delta^{13}C$ excursion as well as Ni isotope anomalies that may record this initial phase of eruptions impacting the terrestrial environment [125]. This region also shows early marine stress [161,162], while more equitorial records show no marine impacts.

The marine extinction interval has a clear, temporal link with the second mostly intrusive phase of the STLIP and gas emissions, and persisted for <100 kyrs straddling the PTB. There were two pulses of extinction intensity at the beginning and end of this interval although significant losses were also occurring in the interlude interval too.

Taxonomic, morphologic, and ecologic selectivity (Fig. 3) and the magnitude of marine extinction suggest that a combination of global warming, anoxia, and oceanic acidification best explains the marine PTME (Fig. 6). Groups intolerant to hypoxia and high temperature were preferentially eliminated during the PTME, suggesting that these stressors played an important role in the extinction of marine animals [157,207] (Fig. 3). Physiologically buffered taxa experienced lower extinction rates than unbuffered taxa [42–44] (Fig. 3). Oceanic acidification could have been an important stressor for shelled animals [43], as also supported by the preferential extinction of coarsely ornamented ammonoids [194] (Fig. 3). Survival animals migrated to higher latitudes or deep seawaters, possibly to escape the hot temperature in equatorial regions or surface seawaters [56,148,156] (Fig. 6).

Summary and future directions

The link between the PTME and the eruption of the STLIP has been well established since the late 1990s 17. Dramatically improved absolute dating has strengthened the link to the point where scenarios involving distinct stages of the emplacement history can be linked with consequent environmental changes (Fig. 6). The effects of the eruptions were likely experienced first in terrestrial settings, where plant productivity crashed and coal ceased to form, and in high-latitudes marine settings in the northern hemisphere. The initial explosive phase of the STLIP emplacement may have driven this crisis, inlcuding increased seasonality, ozone depletion, with higher UV-B radiation, and acid rain.

The marine mass extinction is coeval with the mainly intrusive phase of the STLIP. Increasing fossil and geochemical data resolution indicates that the marine mass extinction could have happened either in two distinct pulses or gradually within an interval straddling the PTB. The thermogenic gases produced by the interaction of magma with the intruded sediments introduced into the PTB atmosphere–ocean system triggered a rapid temperature rise, a decline in ocean ventilation, and ocean acidification, which led to the mass extinction. However, despite the large amount of available data and significantly improved gochronology, the reconstruction of the complex co-occurring phenomena interlinked in the fatal cascade that drove the PTME remains difficult.

Future research direction should aim at improving the spatial and temporal resolution of datasets from PTME terrestrial records. High-precision U-Pb dating of ash beds and detrital zircons, together with magnetostratigraphy and chemostratigraphy, will increase the chronological constraints of the terrestrial crisis, clarifying the delay between the beginning of the extinction on land and in the ocean.

Improved spatial coverage of high-precision stratigraphic syntheses will further evaluate extinction pattern heterogeneity.

Detailed evaluation of PTME palynological assemblages will give a more comprehensive picture of through-ranging taxa to understand dynamics and composition of upland “refugial” or survivor floras. The occurrence of teratologies in sporomorphs must be studied in different plants groups, at different latitudes and throughout the PTME, to identify their ultimate cause and understand whether it interested worlwide flora, and at which stages of the event. Further S-isotope and biomarker analysis of PTME terrestrial successions could strengthen the evidence of acid rains during the terrestrial extinction interval.

The temporal relationship between warming and extinction, both on land and on the ocean, remains problematic, and further studies, including modelling, should try to understand the apparent lags between the C-isotope, O-isotope, and fossil records. Future high-resolution studies ($\delta^{18}O$ from conodont apatite or brachiopod shells) will be pivotal in detecting brief temperature changes on the already manifest long-term CO_2-driven warming trend. However, the current limitation is not the precision of $\delta^{18}O$ analysis but sample availablity. Higher resolution can only be achieved by decreasing the size of conodont samples taken in the field followed by SIMS analyses of individual conodont elements.

Further ecological and physiological studies are required to link environmental changes and extinction patterns. Quantitative predictions for extinction selectivity under different changing environmental conditions are needed to distinguish among potential killing stressors. More consistent geochemical ($\delta^{11}B$) and palaeontological records of ocean saturation are necessary to properly investigate the role of ocean acidification.

Furthermore, future endeavours from the geochronology community should be focused on shedding more light on the temporal correlations between the intrusive and effusive realms of the STLIP, which are still weak. Moreover, since most of the STLIP deposits are covered, it is difficult to fully assess the true nature of the eruption history. Drilling programs could significantly expand the knowledge on the history of the STLIP emplacement. The voluminous tephra deposits and the explosive pipes are tangible proof of explosive activity of the STLIP and of gas discharge to the atmosphere. Clarifying the origin and timing of emplacement of these products and structures would contribute greatly to understanding the link between STLIP emplacement stages and global environmental changes.

Perhaps the most overriding question from the study of mass extinctions driven by volcanic emissions, of which the PTME is the key example, is what can it tells us about future climate trends. Clearly, extreme global warming can lead to severe consequences for the life but if these effects lie tens of

thousands of years in the future, then they are of no geopolitical concern. If changes occur over decades or centuries then their significance increases. Despite the great advances in resolving the details of the PTME, future studies of the crisis should attempt to decipher rates of change on 100–1000 year scale.

References

1. Wignall, P. B. *The Worst of Times*. (Princeton University Press, 2015). doi:10.1515/9781400874248.
2. Song, H. *et al.* Thresholds of temperature change for mass extinctions. *Nature Communications* **12**, 4694 (2021).
3. Jin, Y. G. *et al.* Pattern of marine mass extinction near the Permian-Triassic boundary in South China. *Science* **289**, 432–436 (2000).
4. Song, H., Wignall, P. B., Tong, J. & Yin, H. Two pulses of extinction during the Permian-Triassic crisis. *Nature Geoscience* **6**, 52–56 (2013).
5. Stanley, S. M. Estimates of the magnitudes of major marine mass extinctions in earth history. *Proceedings of the National Academy of Sciences of the United States of America* **113**, E6325–E6334 (2016).
6. Benton, M. J. & Newell, A. J. Impacts of global warming on Permo-Triassic terrestrial ecosystems. *Gondwana Research* **25**, 1308–1337 (2014).
7. Brayard, A. *et al.* Transient metazoan reefs in the aftermath of the end-Permian mass extinction. *Nature Geoscience* **4**, 693–697 (2011).
8. Brayard, A. *et al.* Good genes and good luck: Ammonoid diversity and the end-permian mass extinction. *Science* **325**, 1118–1121 (2009).
9. Scheyer, T. M., Romano, C., Jenks, J. & Bucher, H. Early triassic marine biotic recovery: The predators' perspective. *PLoS ONE* vol. 9 e88987 (2014).
10. Retallack, G. J., Veevers, J. J. & Morante, R. Global coal gap between Permian-Triassic extinction and Middle Triassic recovery of peat-forming plants. *Bulletin of the Geological Society of America* **108**, 195–207 (1996).
11. Payne, J. L. *et al.* Large perturbations of the carbon cycle during recovery from the end-Permian extinction. *Science* **305**, 506–509 (2004).
12. Song, H., Wignall, P. B. & Dunhill, A. M. Decoupled taxonomic and ecological recoveries from the Permo-Triassic extinction. *Science Advances* **4**, eaat5091 (2018).
13. Retallack, G. J. Postapocalyptic greenhouse paleoclimate revealed by earliest Triassic paleosols in the Sydney Basin, Australia. *Bulletin of the Geological Society of America* **111**, 52–70 (1999).
14. Ward, P. D., Montgomery, D. R. & Smith, R. Altered river morphology in South Africa related to the Permian-Triassic extinction. *Science* **289**, 1740–1743 (2000).
15. Wignall, P. B. & Twitchett, R. J. Extent, duration, and nature of the Permian-Triassic superanoxic event. *Special Paper of the Geological Society of America* **356**, 395–413 (2002).
16. Rampino, M. R. & Stothers, R. B. Flood basalt volcanism during the past 250 million years. *Science* **241**, 663–668 (1988).
17. Renne, P. R. & Basu, A. R. Rapid eruption of the Siberian traps flood basalts at the permo-triassic boundary. *Science* **253**, 176–179 (1991).

18. Burgess, S. D. & Bowring, S. A. High-precision geochronology confirms voluminous magmatism before, during, and after Earth's most severe extinction. *Science Advances* **1**, e1500470 (2015).
19. Vasiljev, Y. R., Zolotukhin, V. V., Feoktistov, G. D. & Prusskaya, S. N. Volume estimation and genesis of Permian-Triassic trap magmatism from Siberian platform. *Russian Geology and Geophysics* **41**, 1696–1705 (2000).
20. Dobretsov, N. L. Large igneous provinces of Asia (250 Ma): Siberian and Emeishan traps (plateau basalts) and associated granitoids. *Geologiya i Geofizika* **46**, 870–890 (2005).
21. Augland, L. E. *et al.* The main pulse of the Siberian Traps expanded in size and composition. *Scientific Reports* **9**, 18723 (2019).
22. Kasbohm, J., Schoene, B. & Burgess, S. Radiometric Constraints on the Timing, Tempo, and Effects of Large Igneous Province Emplacement. in *Large Igneous Provinces: A Driver of Global Environmental and Biotic Changes* 27–82 (2021). doi:10.1002/9781119507444.ch2.
23. Burgess, S. D., Muirhead, J. D. & Bowring, S. A. Initial pulse of Siberian Traps sills as the trigger of the end-Permian mass extinction. *Nature Communications* **8**, 164 (2017).
24. Posenato, R. Marine biotic events in the lopingian succession and latest Permian extinction in the Southern Alps (Italy). *Geological Journal* **45**, 195–215 (2010).
25. Posenato, R. The end-Permian mass extinction (EPME) and the early triassic biotic recovery in the western Dolomites (Italy): state of the art. *Bollettino della Societa Paleontologica Italiana* **58**, 11–34 (2019).
26. Fielding, C. R. *et al.* Age and pattern of the southern high-latitude continental end-Permian extinction constrained by multiproxy analysis. *Nature Communications* **10**, 385 (2019).
27. Chu, D. *et al.* Ecological disturbance in tropical peatlands prior to marine Permian-Triassic mass extinction. *Geology* **48**, 288–292 (2020).
28. Gastaldo, R. A. *et al.* The base of the Lystrosaurus Assemblage Zone, Karoo Basin, predates the end-Permian marine extinction. *Nature Communications* **11**, 1428 (2020).
29. Foote, M. Morphological and taxonomic diversity in clade's history: the blastoid record and stochastic simulations. *Contributions From the Museum of Paleontology* **28**, 101–140 (1991).
30. Stanley, S. M. & Yang, X. A double mass extinction at the end of the paleozoic era. *Science* **266**, 1340–1344 (1994).
31. Wang, X. D. & Sugiyama, T. Diversity and extinction patterns of Permian coral faunas of China. *Lethaia* **33**, 285–294 (2000).
32. Hallam, A. & Wignall, P. B. *Mass Extinctions and their Aftermath*. (Oxford University Press, 1997).
33. Orchard, M. J. Conodont diversity and evolution through the latest Permian and Early Triassic upheavals. *Palaeogeography, Palaeoclimatology, Palaeoecology* **252**, 93–117 (2007).
34. Romano, C. *et al.* Permian-Triassic Osteichthyes (bony fishes): Diversity dynamics and body size evolution. *Biological Reviews* **91**, 106–147 (2016).
35. Tu, C., Chen, Z. Q. & Harper, D. A. T. Permian–Triassic evolution of the Bivalvia: Extinction-recovery patterns linked to ecologic and taxonomic selectivity. *Palaeogeography, Palaeoclimatology, Palaeoecology* **459**, 53–62 (2016).
36. Schaal, E. K., Clapham, M. E., Rego, B. L., Wang, S. C. & Payne, J. L. Comparative size evolution of marine clades from the Late Permian through Middle Triassic. *Paleobiology* **42**, 127–142 (2016).

37. Chen, J. *et al.* Size variation of brachiopods from the Late Permian through the Middle Triassic in South China: Evidence for the Lilliput Effect following the Permian-Triassic extinction. *Palaeogeography, Palaeoclimatology, Palaeoecology* **519**, 248–257 (2019).
38. Feng, Y., Song, H. & Bond, D. P. G. Size variations in foraminifers from the early Permian to the Late Triassic: Implications for the Guadalupian-Lopingian and the Permian-Triassic mass extinctions. *Paleobiology* **46**, 511–532 (2020).
39. Luo, G., Lai, X., Jiang, H. & Zhang, K. Size variation of the end Permian conodont Neogondolella at Meishan Section, Changxing, Zhejiang and its significance. *Science in China, Series D: Earth Sciences* **49**, 337–347 (2006).
40. Brayard, A. *et al.* Early Triassic Gulliver gastropods: Spatio-temporal distribution and significance for biotic recovery after the end-Permian mass extinction. *Earth-Science Reviews* vol. 146 31–64 (2015).
41. Knoll, A. H., Bambach, R. K., Canfield, D. E. & Grotzinger, J. P. Comparative earth history and late Permian mass extinction. *Science* vol. 273 452–457 (1996).
42. Knoll, A. H., Bambach, R. K., Payne, J. L., Pruss, S. & Fischer, W. W. Paleophysiology and end-Permian mass extinction. *Earth and Planetary Science Letters* **256**, 295–313 (2007).
43. Clapham, M. E. & Payne, J. L. Acidification, anoxia, and extinction: A multiple logistic regression analysis of extinction selectivity during the Middle and Late Permian. *Geology* **39**, 1059–1062 (2011).
44. Vázquez, P. & Clapham, M. E. Extinction selectivity among marine fishes during multistressor global change in the end-Permian and end-Triassic crises. *Geology* **45**, 395–398 (2017).
45. Payne, J. L. & Finnegan, S. The effect of geographic range on extinction risk during background and mass extinction. *Proceedings of the National Academy of Sciences of the United States of America* **104**, 10506–10511 (2007).
46. Dai, X. & Song, H. Toward an understanding of cosmopolitanism in deep time: A case study of ammonoids from the middle Permian to the Middle Triassic. *Paleobiology* **46**, 533–549 (2020).
47. Kiessling, W. *et al.* Pre-mass extinction decline of latest Permian ammonoids. *Geology* **46**, 283–286 (2018).
48. Rampino, M. R. & Adler, A. C. Evidence for abrupt latest Permian mass extinction of foraminifera: results of tests for the Signor-Lipps effect. *Geology* **26**, 415–418 (1998).
49. Song, H., Tong, J., Chen, Z. Q., Yang, H. & Wang, Y. End-Permian mass extinction of foraminifers in the Nanpanjiang basin, South China. *Journal of Paleontology* **83**, 718–738 (2009).
50. Wignall, P. B. & Hallam, A. Anoxia as a cause of the Permian/Triassic mass extinction: facies evidence from northern Italy and the western United States. *Palaeogeography, Palaeoclimatology, Palaeoecology* **93**, 21–46 (1992).
51. Shen, S. Z. *et al.* A sudden end-Permian mass extinction in South China. *Bulletin of the Geological Society of America* **131**, 205–223 (2019).
52. Angiolini, L., Checconi, A., Gaetani, M. & Rettori, R. The latest Permian mass extinction in the Alborz Mountains (North Iran). *Geological Journal* **45**, 216–229 (2010).
53. Yin, H., Feng, Q., Lai, X., Baud, A. & Tong, J. The protracted Permo-Triassic crisis and multi-episode extinction around the Permian-Triassic boundary. *Global and Planetary Change* **55**, 1–20 (2007).

54. Wignall, P. B. & Newton, R. Contrasting deep-water records from the Upper Permian and Lower Triassic of South Tibet and British Columbia: Evidence for a diachronous mass extinction. *Palaios* **18**, 153–167 (2003).
55. Wang, Y. *et al.* Quantifying the process and abruptness of the end-Permian mass extinction. *Paleobiology* **40**, 113–129 (2014).
56. Liu, X., Song, H., Bond, D. P. G., Tong, J. & Benton, M. J. Migration controls extinction and survival patterns of foraminifers during the Permian-Triassic crisis in South China. *Earth-Science Reviews* vol. 209 103329 (2020).
57. Chen, Z. Q. *et al.* Environmental and biotic turnover across the Permian-Triassic boundary on a shallow carbonate platform in western Zhejiang, South China. *Australian Journal of Earth Sciences* **56**, 775–797 (2009).
58. He, W. H. *et al.* Late Permian marine ecosystem collapse began in deeper waters: Evidence from brachiopod diversity and body size changes. *Geobiology* **13**, 123–138 (2015).
59. Burgess, S. D., Bowring, S. & Shen, S. Z. High-precision timeline for Earth's most severe extinction. *Proceedings of the National Academy of Sciences of the United States of America* **111**, 3316–3321 (2014).
60. Yang, H. *et al.* Composition and structure of microbialite ecosystems following the end-Permian mass extinction in South China. *Palaeogeography, Palaeoclimatology, Palaeoecology* **308**, 111–128 (2011).
61. Tian, L. *et al.* Distribution and size variation of ooids in the aftermath of the permian-triassic mass extinction. *Palaios* **30**, 714–727 (2015).
62. Retallack, G. J. Permian-triassic life crisis on land. *Science* **267**, 77–80 (1995).
63. Looy, C. V., Brugman, W. A., Dilcher, D. L. & Visscher, H. The delayed resurgence of equatorial forests after the Permian-Triassic ecologic crisis. *Proceedings of the National Academy of Sciences of the United States of America* **96**, 13857–13862 (1999).
64. Hermann, E. *et al.* Terrestrial ecosystems on North Gondwana following the end-Permian mass extinction. *Gondwana Research* **20**, 630–637 (2011).
65. Cascales-Miñana, B., Diez, J. B., Gerrienne, P. & Cleal, C. J. A palaeobotanical perspective on the great end-Permian biotic crisis. *Historical Biology* **28**, 1066–1074 (2016).
66. Yu, J. *et al.* Vegetation changeover across the Permian-Triassic Boundary in Southwest China. Extinction, survival, recovery and palaeoclimate: A critical review. *Earth-Science Reviews* vol. 149 203–224 (2015).
67. Vajda, V. *et al.* End-Permian (252 Mya) deforestation, wildfires and flooding—An ancient biotic crisis with lessons for the present. *Earth and Planetary Science Letters* **529**, 115875 (2020).
68. Schneebeli-Hermann, E., Hochuli, P. A. & Bucher, H. Palynofloral associations before and after the Permian–Triassic mass extinction, Kap Stosch, East Greenland. *Global and Planetary Change* **155**, 178–195 (2017).
69. Nowak, H., Schneebeli-Hermann, E. & Kustatscher, E. No mass extinction for land plants at the Permian–Triassic transition. *Nature Communications* **10**, 384 (2019).
70. Chu, D. *et al.* Biostratigraphic correlation and mass extinction during the Permian-Triassic transition in terrestrial-marine siliciclastic settings of South China. *Global and Planetary Change* **146**, 67–88 (2016).
71. Zhang, H. *et al.* The terrestrial end-Permian mass extinction in South China. *Palaeogeography, Palaeoclimatology, Palaeoecology* **448**, 108–124 (2016).

72. Krassilov, V. & Karasev, E. Paleofloristic evidence of climate change near and beyond the Permian-Triassic boundary. *Palaeogeography, Palaeoclimatology, Palaeoecology* **284**, 326–336 (2009).
73. Mcloughlin, S., Lindström, S. & Drinnan, A. N. Gondwanan floristic and sedimentological trends during the Permian-Triassic transition: New evidence from the Amery Group, northern Prince Charles Mountains, East Antarctica. *Antarctic Science* **9**, 281–298 (1997).
74. Kerp, H., Hamad, A. A., Vörding, B. & Bandel, K. Typical Triassic Gondwanan floral elements in the Upper Permian of the paleotropics. *Geology* **34**, 265–268 (2006).
75. Eshet, Y., Rampino, M. R. & Visscher, H. Fungal event and palynological record of ecological crisis and recovery across the Permian-Triassic boundary. *Geology* **23**, 967–970 (1995).
76. Visscher, H. *et al.* Environmental mutagenesis during the end-Permian ecological crisis. *Proceedings of the National Academy of Sciences of the United States of America* **101**, 12952–12956 (2004).
77. Looy, C. V., Collinson, M. E., Van Konijnenburg-Van Cittert, J. H. A., Visscher, H. & Brain, A. P. R. The ultrastructure and botanical affinity of end-permian spore tetrads. *International Journal of Plant Sciences* **166**, 875–887 (2005).
78. Foster, C. B. & Afonin, S. A. Abnormal pollen grains: An outcome of deteriorating atmospheric conditions around the Permian-Triassic boundary. *Journal of the Geological Society* **162**, 653–659 (2005).
79. Hochuli, P. A., Schneebeli-Hermann, E., Mangerud, G. & Bucher, H. Evidence for atmospheric pollution across the Permian-Triassic transition. *Geology* **45**, 1123–1126 (2017).
80. Rampino, M. R. & Eshet, Y. The fungal and acritarch events as time markers for the latest Permian mass extinction: An update. *Geoscience Frontiers* **9**, 147–154 (2018).
81. Benca, J. P., Duijnstee, I. A. P. & Looy, C. V. UV-B–induced forest sterility: Implications of ozone shield failure in earth's largest extinction. *Science Advances* **4**, (2018).
82. Chu, D. *et al.* Metal-induced stress in survivor plants following the end-Permian collapse of land ecosystems. *Geology* **49**, 657–661 (2021).
83. Schneebeli-Hermann, E. *et al.* Vegetation history across the Permian-Triassic boundary in Pakistan (Amb section, Salt Range). *Gondwana Research* **27**, 911–924 (2015).
84. Visscher, H. *et al.* The terminal paleozoic fungal event: Evidence of terrestrial ecosystem destabilization and collapse. *Proceedings of the National Academy of Sciences of the United States of America* **93**, 2155–2158 (1996).
85. Visscher, H., Sephton, M. A. & Looy, C. V. Fungal virulence at the time of the end-Permian biosphere crisis? *Geology* **39**, 883–886 (2011).
86. Looy, C. V., Twitchett, R. J., Dilcher, D. L., Van Konijnenburg-Van Cittert, J. H. A. & Visscher, H. Life in the end-Permian dead zone. *Proceedings of the National Academy of Sciences of the United States of America* **98**, 7879–7883 (2001).
87. Bercovici, A. & Vajda, V. Terrestrial Permian - Triassic boundary sections in South China. *Global and Planetary Change* **143**, 31–33 (2016).
88. Hochuli, P. A. Interpretation of "fungal spikes" in Permian-Triassic boundary sections. *Global and Planetary Change* **144**, 48–50 (2016).
89. Angielczyk, K. D., Roopnarine, P. D. & Wang, S. C. Modeling the role of primary productivity disruption in end-Permian extinctions. *New Mexico Museum of Natural History and Science Bulletin* **30**, 16–23 (2005).

90. Labandeira, C. C. & Sepkoski, J. J. Insect diversity in the fossil record. *Science* **261**, 310–315 (1993).
91. Shcherbakov, D. E. On Permian and Triassic insect faunas in relation to biogeography and the Permian-Triassic crisis. *Paleontological Journal* **42**, 15–31 (2008).
92. Condamine, F. L., Clapham, M. E. & Kergoat, G. J. Global patterns of insect diversification: Towards a reconciliation of fossil and molecular evidence? *Scientific Reports* **6**, 19208 (2016).
93. Smith, R. M. H. & Ward, P. D. Pattern of vertebrate extinctions across an event bed at the Permian-Triassic boundary in the Karoo Basin of South Africa. *Geology* **29**, 1147 (2001).
94. Benton, M. J., Tverdokhlebov, V. P. & Surkov, M. V. Ecosystem remodelling among vertebrates at the Permian-Triassic boundary in Russia. *Nature* **432**, 97–100 (2004).
95. Viglietti, P. A. *et al.* Evidence from South Africa for a protracted end-Permian extinction on land. *Proceedings of the National Academy of Sciences of the United States of America* **118**, e2017045118 (2021).
96. Sennikov, A. G. & Golubev, V. K. Vyazniki biotic assemblage of the terminal Permian. *Paleontological Journal* **40**, S475–S481 (2006).
97. Sennikov, A. G. & Golubev, V. K. On the faunal verification of the Permo-Triassic boundary in continental deposits of eastern Europe: 1. Gorokhovets-Zhukov ravine. *Paleontological Journal* **46**, 313–323 (2012).
98. Zhu, Z. *et al.* Altered fluvial patterns in North China indicate rapid climate change linked to the Permian-Triassic mass extinction. *Scientific Reports* **9**, 16818 (2019).
99. Shen, S. Z. *et al.* Calibrating the end-Permian mass extinction. *Science* **334**, 1367–1372 (2011).
100. Twitchett, R. J., Looy, C. V., Morante, R., Visscher, H. & Wignall, P. B. Rapid and synchronous collapse of marine and terrestrial ecosystems during the end-Permian biotic crisis. *Geology* **29**, 351–354 (2001).
101. Biswas, R. K., Kaiho, K., Saito, R., Tian, L. & Shi, Z. Terrestrial ecosystem collapse and soil erosion before the end-Permian marine extinction: Organic geochemical evidence from marine and non-marine records. *Global and Planetary Change* **195**, 103327 (2020).
102. Aftabuzzaman, Md. *et al.* End-Permian terrestrial disturbance followed by the complete plant devastation, and the vegetation proto-recovery in the earliest-Triassic recorded in coastal sea sediments. *Global and Planetary Change* **205**, 103621 (2021).
103. Gastaldo, R. A., Neveling, J., Geissman, J. W., Kamo, S. L. & Looy, C. V. A tale of two Tweefonteins: What physical correlation, geochronology, magnetic polarity stratigraphy, and palynology reveal about the end-Permian terrestrial extinction paradigm in South Africa. *GSA Bulletin* (2021) doi:10.1130/b35830.1.
104. Yan, Z. *et al.* Frequent and intense fires in the final coals of the Paleozoic indicate elevated atmospheric oxygen levels at the onset of the End-Permian Mass Extinction Event. *International Journal of Coal Geology* **207**, 75–83 (2019).
105. DiMichele, W. A., Bashforth, A. R., Falcon-Lang, H. J. & Lucas, S. G. Uplands, lowlands, and climate: Taphonomic megabiases and the apparent rise of a xeromorphic, drought-tolerant flora during the Pennsylvanian-Permian transition. *Palaeogeography, Palaeoclimatology, Palaeoecology* **559**, 109965 (2020).
106. Smith, R. M. H. & Botha-Brink, J. Anatomy of a mass extinction: Sedimentological and taphonomic evidence for drought-induced die-offs at the Permo-Triassic boundary in the main Karoo Basin, South Africa. *Palaeogeography, Palaeoclimatology, Palaeoecology* **396**, 99–118 (2014).

107. Xiong, C. & Wang, Q. Permian–Triassic land-plant diversity in South China: Was there a mass extinction at the Permian/Triassic boundary? *Paleobiology* **37**, 157–167 (2011).
108. Yu, J. *et al.* Terrestrial events across the Permian-Triassic boundary along the Yunnan-Guizhou border, SW China. *Global and Planetary Change* **55**, 193–208 (2007).
109. Becker, L., Poreda, R. J., Hunt, A. G., Bunch, T. E. & Rampino, M. Impact event at the permian-triassic boundary: Evidence from extraterrestrial noble gases in fullerenes. *Science* **291**, 1530–1533 (2001).
110. Basu, A. R., Petaev, M. I., Poreda, R. J., Jacobsen, S. B. & Becker, L. Chondritic Meteorite Fragments Associated with the Permian-Triassic Boundary in Antarctica. *Science* **302**, 1388–1392 (2003).
111. Isozaki, Y. Permo-Triassic boundary superanoxia and stratified superocean: Records from lost deep sea. *Science* **276**, 235–238 (1997).
112. French, B. M. & Koeberl, C. The convincing identification of terrestrial meteorite impact structures: What works, what doesn't, and why. *Earth-Science Reviews* vol. 98 123–170 (2010).
113. Saunders, A. D., England, R. W., Reichow, M. K. & White, R. V. A mantle plume origin for the Siberian traps: Uplift and extension in the West Siberian Basin, Russia. *Lithos* **79**, 407–424 (2005).
114. Reichow, M. K. *et al.* Petrogenesis and timing of mafic magmatism, South Taimyr, Arctic Siberia: A northerly continuation of the Siberian Traps? *Lithos* **248–251**, 382–401 (2016).
115. Naldrett, A. J., Lightfoot, P. C., Fedorenko, V., Doherty, W. & Gorbachev, N. S. Geology and geochemistry of intrusions and flood basalts of the Noril'sk region, USSR, with implications for the origin of the Ni-Cu ores. *Economic Geology* **87**, 975–1004 (1992).
116. Hawkesworth, C. J. *et al.* Magma differentiation and mineralisation in the Siberian continental flood basalts. *LITHOS* **34**, 61–88 (1995).
117. Fedorenko, V. A. *et al.* Petrogenesis of the flood-basalt sequence at noril'sk, north central siberia. *International Geology Review* **38**, 99–135 (1996).
118. Arndt, N., Chauvel, C., Czamanske, G. & Fedorenko, V. Two mantle sources, two plumbing systems: Tholeiitic and alkaline magmatism of the Maymecha River basin, Siberian flood volcanic province. *Contributions to Mineralogy and Petrology* **133**, 297–313 (1998).
119. Sobolev, S. V. *et al.* Linking mantle plumes, large igneous provinces and environmental catastrophes. *Nature* **477**, 312–316 (2011).
120. Sobolev, A. V., Arndt, N. T., Krivolutskaya, N. A., Kuzmin, D. V. & Sobolev, S. V. The origin of gases that caused the permian-triassic extinction. in *Volcanism and Global Environmental Change* 147–163 (2015). doi:10.1007/9781107415683.011.
121. Black, B. A., Elkins-Tanton, L. T., Rowe, M. C. & Peate, I. U. Magnitude and consequences of volatile release from the Siberian Traps. *Earth and Planetary Science Letters* **317–318**, 363–373 (2012).
122. Broadley, M. W., Barry, P. H., Ballentine, C. J., Taylor, L. A. & Burgess, R. End-Permian extinction amplified by plume-induced release of recycled lithospheric volatiles. *Nature Geoscience* **11**, 682–687 (2018).
123. Elkins-Tanton, L. T. *et al.* Field evidence for coal combustion links the 252 Ma Siberian Traps with global carbon disruption. *Geology* **48**, 986–991 (2020).
124. Grasby, S. E. & Beauchamp, B. Latest Permian to Early Triassic basin-to-shelf anoxia in the Sverdrup Basin, Arctic Canada. *Chemical Geology* **264**, 232–246 (2009).

125. Grasby, S. E., Sanei, H. & Beauchamp, B. Catastrophic dispersion of coal fly ash into oceans during the latest Permian extinction. *Nature Geoscience* **4**, 104–107 (2011).
126. Sanei, H., Grasby, S. E. & Beauchamp, B. Latest permian mercury anomalies. *Geology* **40**, 63–66 (2012).
127. Reichow, M. K., Saunders, A. D., White, R. V., Al'Mukhamedov, A. I. & Medvedev, A. Y. Geochemistry and petrogenesis of basalts from the West Siberian Basin: An extension of the Permo-Triassic Siberian Traps, Russia. *Lithos* **79**, 425–452 (2005).
128. Jerram, D. A., Svensen, H. H., Planke, S., Polozov, A. G. & Torsvik, T. H. The onset of flood volcanism in the north-western part of the Siberian Traps: Explosive volcanism versus effusive lava flows. *Palaeogeography, Palaeoclimatology, Palaeoecology* **441**, 38–50 (2016).
129. Svensen, H. *et al.* Siberian gas venting and the end-Permian environmental crisis. *Earth and Planetary Science Letters* **277**, 490–500 (2009).
130. Svensen, H. H. *et al.* Sills and gas generation in the Siberian Traps. *Philosophical Transactions of the Royal Society A: Mathematical, Physical and Engineering Sciences* **376**, 20170080 (2018).
131. Davydov, V. I. Tunguska coals, Siberian sills and the Permian-Triassic extinction. *Earth-Science Reviews* vol. 212 103438 (2021).
132. Callegaro, S. *et al.* Geochemistry of deep Tunguska Basin sills, Siberian Traps: correlations and potential implications for the end-Permian environmental crisis. *Contributions to Mineralogy and Petrology* **176**, 49 (2021).
133. Wooden, J. L. *et al.* Isotopic and trace-element constraints on mantle and crustal contributions to Siberian continental flood basalts, Noril'sk area, Siberia. *Geochimica et Cosmochimica Acta* **57**, 3677–3704 (1993).
134. Arndt, N. T., Czmanske, G. K., Walker, R. J., Chauvel, C. & Fedorenko, V. A. Geochemistry and origin of the intrusive hosts of the Noril'sk-Talnakh Cu-Ni-PGE sulfide deposits. *Economic Geology* **98**, 495–515 (2003).
135. Pang, K. N. *et al.* A petrologic, geochemical and Sr-Nd isotopic study on contact metamorphism and degassing of Devonian evaporites in the Norilsk aureoles, Siberia. *Contributions to Mineralogy and Petrology* **165**, 683–704 (2013).
136. Yao, Z. sen & Mungall, J. E. Linking the Siberian Flood Basalts and Giant Ni-Cu-PGE Sulfide Deposits at Norilsk. *Journal of Geophysical Research: Solid Earth* **126**, (2021).
137. Sibik, S., Edmonds, M., Maclennan, J. & Svensen, H. Magmas Erupted during the Main Pulse of Siberian Traps Volcanism were Volatile-poor. *Journal of Petrology* **56**, 2089–2116 (2015).
138. Retallack, G. J. & Jahren, A. H. Methane release from igneous intrusion of coal during late permian extinction events. *Journal of Geology* **116**, 1–20 (2008).
139. Iacono-Marziano, G. *et al.* Gas emissions due to magma-sediment interactions during flood magmatism at the Siberian Traps: Gas dispersion and environmental consequences. *Earth and Planetary Science Letters* **357–358**, 308–318 (2012).
140. Fristad, K. E., Svensen, H. H., Polozov, A. & Planke, S. Formation and evolution of the end-Permian Oktyabrsk volcanic crater in the Tunguska Basin, Eastern Siberia. *Palaeogeography, Palaeoclimatology, Palaeoecology* **468**, 76–87 (2017).
141. Polozov, A. G. *et al.* The basalt pipes of the Tunguska Basin (Siberia, Russia): High temperature processes and volatile degassing into the end-Permian atmosphere. *Palaeogeography, Palaeoclimatology, Palaeoecology* **441**, 51–64 (2016).
142. Elkins-Tanton, L. T. *et al.* The last lavas erupted during the main phase of the Siberian flood volcanic province: Results from experimental petrology. *Contributions to Mineralogy and Petrology* **153**, 191–209 (2007).

143. Schmidt, A. *et al.* Selective environmental stress from sulphur emitted by continental flood basalt eruptions. *Nature Geoscience* **9**, 77–82 (2016).
144. Black, B. A. *et al.* Systemic swings in end-Permian climate from Siberian Traps carbon and sulfur outgassing. *Nature Geoscience* **11**, 949–954 (2018).
145. Schobben, M., Joachimski, M. M., Korn, D., Leda, L. & Korte, C. Palaeotethys seawater temperature rise and an intensified hydrological cycle following the end-Permian mass extinction. *Gondwana Research* **26**, 675–683 (2014).
146. Chen, J. *et al.* Abrupt warming in the latest Permian detected using high-resolution in situ oxygen isotopes of conodont apatite from Abadeh, central Iran. *Palaeogeography, Palaeoclimatology, Palaeoecology* **560**, 109973 (2020).
147. Joachimski, M. M., Alekseev, A. S., Grigoryan, A. & Gatovsky, Y. A. Siberian trap volcanism, global warming and the Permian-Triassic mass extinction: New insights from Armenian Permian-Triassic sections. *Bulletin of the Geological Society of America* **132**, 427–443 (2020).
148. Sun, Y. *et al.* Lethally hot temperatures during the early triassic greenhouse. *Science* **338**, 366–370 (2012).
149. Joachimski, M. M. *et al.* Climate warming in the latest Permian and the Permian-Triassic mass extinction. *Geology* **40**, 195–198 (2012).
150. Jiang, H., Joachimski, M. M., Wignall, P. B., Zhang, M. & Lai, X. A delayed end-Permian extinction in deep-water locations and its relationship to temperature trends (Bianyang, Guizhou Province, South China). *Palaeogeography, Palaeoclimatology, Palaeoecology* **440**, 690–695 (2015).
151. Chen, J. *et al.* High-resolution SIMS oxygen isotope analysis on conodont apatite from South China and implications for the end-Permian mass extinction. *Palaeogeography, Palaeoclimatology, Palaeoecology* **448**, 26–38 (2016).
152. Shen, S. *et al.* Permian integrative stratigraphy and timescale of China. *Science China Earth Sciences* vol. 62 154–188 (2019).
153. Pörtner, H. O. Oxygen- And capacity-limitation of thermal tolerance: A matrix for integrating climate-related stressor effects in marine ecosystems. *Journal of Experimental Biology* **213**, 881–893 (2010).
154. Pörtner, H. O. Integrating climate-related stressor effects on marine organisms: Unifying principles linking molecule to ecosystem-level changes. *Marine Ecology Progress Series* **470**, 273–290 (2012).
155. Bijma, J., Pörtner, H. O., Yesson, C. & Rogers, A. D. Climate change and the oceans - What does the future hold? *Marine Pollution Bulletin* **74**, 495–505 (2013).
156. Song, H. *et al.* Flat latitudinal diversity gradient caused by the Permian–Triassic mass extinction. *Proceedings of the National Academy of Sciences of the United States of America* **117**, 17578–17583 (2020).
157. Penn, J. L., Deutsch, C., Payne, J. L. & Sperling, E. A. Temperature-dependent hypoxia explains biogeography and severity of end-Permian marine mass extinction. *Science* **362**, eaat1327 (2018).
158. Benton, M. J. Hyperthermal-driven mass extinctions: Killing models during the Permian-Triassic mass extinction. *Philosophical Transactions of the Royal Society A: Mathematical, Physical and Engineering Sciences* vol. 376 20170076 (2018).
159. Teskey, R. *et al.* Responses of tree species to heat waves and extreme heat events. *Plant Cell and Environment* vol. 38 1699–1712 (2015).
160. Cai, Y. F., Zhang, H., Feng, Z. & Shen, S. Z. Intensive Wildfire Associated With Volcanism Promoted the Vegetation Changeover in Southwest China During the Permian−Triassic Transition. *Frontiers in Earth Science* **9**, 615841 (2021).

161. Grasby, S. E. *et al.* Progressive environmental deterioration in northwestern Pangea leading to the latest Permian extinction. *Bulletin of the Geological Society of America* **127**, 1331–1347 (2015).
162. Beauchamp, B. & Grasby, S. E. Permian lysocline shoaling and ocean acidification along NW Pangea led to carbonate eradication and chert expansion. *Palaeogeography, Palaeoclimatology, Palaeoecology* **350–352**, 73–90 (2012).
163. Wignall, P. B. & Twitchett, R. J. Oceanic anoxia and the end permian mass extinction. *Science* **272**, 1155–1158 (1996).
164. Wignall, P. B. *et al.* Ultra-shallow-marine anoxia in an Early Triassic shallow-marine clastic ramp (Spitsbergen) and the suppression of benthic radiation. *Geological Magazine* **153**, 316–331 (2016).
165. Proemse, B. C., Grasby, S. E., Wieser, M. E., Mayer, B. & Beauchamp, B. Molybdenum isotopic evidence for oxic marine conditions during the latest permian extinction. *Geology* **41**, 967–970 (2013).
166. Grasby, S. E. *et al.* Transient Permian-Triassic euxinia in the southern Panthalassa deep ocean. *Geology* **49**, 889–893 (2021).
167. Wignall, P. B. *et al.* An 80 million year oceanic redox history from Permian to Jurassic pelagic sediments of the Mino-Tamba terrane, SW Japan, and the origin of four mass extinctions. *Global and Planetary Change* **71**, 109–123 (2010).
168. Song, H. *et al.* Geochemical evidence from bio-apatite for multiple oceanic anoxic events during Permian-Triassic transition and the link with end-Permian extinction and recovery. *Earth and Planetary Science Letters* **353–354**, 12–21 (2012).
169. Grasby, S. E., Beauchamp, B., Embry, A. & Sanei, H. Recurrent Early Triassic ocean anoxia. *Geology* **41**, 175–178 (2013).
170. Takahashi, S., Yamasaki, S. ichi, Ogawa, K., Kaiho, K. & Tsuchiya, N. Redox conditions in the end-Early Triassic Panthalassa. *Palaeogeography, Palaeoclimatology, Palaeoecology* **432**, 15–28 (2015).
171. Brennecka, G. A., Herrmann, A. D., Algeo, T. J. & Anbar, A. D. Rapid expansion of oceanic anoxia immediately before the end-Permian mass extinction. *Proceedings of the National Academy of Sciences of the United States of America* **108**, 17631–17634 (2011).
172. Takahashi, S. *et al.* Bioessential element-depleted ocean following the euxinic maximum of the end-Permian mass extinction. *Earth and Planetary Science Letters* **393**, 94–104 (2014).
173. Newton, R. J., Pevitt, E. L., Wignall, P. B. & Bottrell, S. H. Large shifts in the isotopic composition of seawater sulphate across the Permo-Triassic boundary in northern Italy. *Earth and Planetary Science Letters* **218**, 331–345 (2004).
174. Grice, K. *et al.* Photic zone euxinia during the permian-triassic superanoxic event. *Science* **307**, 706–709 (2005).
175. Ingall, E. & Jahnke, R. Evidence for enhanced phosphorus regeneration from marine sediments overlain by oxygen depleted waters. *Geochimica et Cosmochimica Acta* vol. 58 2571–2575 (1994).
176. Sun, Y. D. *et al.* Ammonium ocean following the end-Permian mass extinction. *Earth and Planetary Science Letters* **518**, 211–222 (2019).
177. Grasby, S. E., Beauchamp, B. & Knies, J. Early Triassic productivity crises delayed recovery from world's worst mass extinction. *Geology* **44**, 779–782 (2016).
178. Schoepfer, S. D., Henderson, C. M., Garrison, G. H. & Ward, P. D. Cessation of a productive coastal upwelling system in the Panthalassic Ocean at the Permian-Triassic Boundary. *Palaeogeography, Palaeoclimatology, Palaeoecology* **313–314**, 181–188 (2012).

179. Schobben, M. *et al.* Flourishing ocean drives the end-Permian marine mass extinction. *Proceedings of the National Academy of Sciences of the United States of America* **112**, 10298–10303 (2015).
180. Grasby, S. E. *et al.* Global warming leads to Early Triassic nutrient stress across northern Pangea. *Bulletin of the Geological Society of America* **132**, 943–954 (2020).
181. Song, H. *et al.* Conodont calcium isotopic evidence for multiple shelf acidification events during the Early Triassic. *Chemical Geology* **562**, (2021).
182. Jurikova, H. *et al.* Permian–Triassic mass extinction pulses driven by major marine carbon cycle perturbations. *Nature Geoscience* **13**, 745–750 (2020).
183. Garbelli, C., Angiolini, L. & Shen, S. Z. Biomineralization and global change: A new perspective for understanding the end-Permian extinction. *Geology* **45**, 19–22 (2017).
184. Clarkson, M. O. *et al.* Ocean acidification and the Permo-Triassic mass extinction. *Science* **348**, 229–232 (2015).
185. Zhang, S. *et al.* Investigating controls on boron isotope ratios in shallow marine carbonates. *Earth and Planetary Science Letters* **458**, 380–393 (2017).
186. Hinojosa, J. L. *et al.* Evidence for end-Permian ocean acidification from calcium isotopes in biogenic apatite. *Geology* **40**, 743–746 (2012).
187. Komar, N. & Zeebe, R. E. Calcium and calcium isotope changes during carbon cycle perturbations at the end-Permian. *Paleoceanography* **31**, 115–130 (2016).
188. Silva-Tamayo, J. C. *et al.* Global perturbation of the marine calcium cycle during the Permian-Triassic transition. *Bulletin of the Geological Society of America* **130**, 1323–1338 (2018).
189. Payne, J. L. *et al.* Calcium isotope constraints on the end-Permian mass extinction. *Proceedings of the National Academy of Sciences of the United States of America* **107**, 8543–8548 (2010).
190. Lau, K. V. *et al.* The influence of seawater carbonate chemistry, mineralogy, and diagenesis on calcium isotope variations in Lower-Middle Triassic carbonate rocks. *Chemical Geology* **471**, 13–37 (2017).
191. Wang, J. *et al.* Coupled δ44/40Ca, δ88/86Sr, and 87Sr/86Sr geochemistry across the end-Permian mass extinction event. *Geochimica et Cosmochimica Acta* **262**, 143–165 (2019).
192. Kiessling, W. & Simpson, C. On the potential for ocean acidification to be a general cause of ancient reef crises. *Global Change Biology* **17**, 56–67 (2011).
193. Chen, Z. Q., Kaiho, K. & George, A. D. Early Triassic recovery of the brachiopod faunas from the end-Permian mass extinction: A global review. in *Palaeogeography, Palaeoclimatology, Palaeoecology* vol. 224 270–290 (2005).
194. Dai, X., Korn, D. & Song, H. Morphological selectivity of the Permian-Triassic ammonoid mass extinction. *Geology* **49**, 1112–1116 (2021).
195. Fijałkowska-Mader, A. Impact of the Environmental Stress on the Late Permian Pollen Grains from Zechstein Deposits of Poland. in *Morphogenesis, Environmental Stress and Reverse Evolution* 23–35 (2020). doi:10.1007/978-3-030-47279-5_3.
196. Beerling, D. J., Harfoot, M., Lomax, B. & Pyle, J. A. The stability of the stratospheric ozone layer during the end-Permian eruption of the Siberian Traps. *Philosophical Transactions of the Royal Society A: Mathematical, Physical and Engineering Sciences* **365**, 1843–1866 (2007).
197. Svensen, H., Schmidbauer, N., Roscher, M., Stordal, F. & Planke, S. Contact metamorphism, halocarbons, and environmental crises of the past. *Environmental Chemistry* **6**, 466–471 (2009).

198. Black, B. A., Lamarque, J. F., Shields, C. A., Elkins-Tanton, L. T. & Kiehl, J. T. Acid rain and ozone depletion from pulsed siberian traps magmatism. *Geology* **42**, 67–70 (2014).
199. Likens, G. E. & Butler, T. J. Acid Rain: Causes, Consequences, and Recovery in Terrestrial, Aquatic, and Human Systems. in *Encyclopedia of the Anthropocene* 23–31 (2018). doi:10.1016/b978-0-12-809665-9.09977-8.
200. Sephton, M. A., Jiao, D., Engel, M. H., Looy, C. V. & Visscher, H. Terrestrial acidification during the end-Permian biosphere crisis? *Geology* **43**, 159–162 (2015).
201. Sheldon, N. D. Abrupt chemical weathering increase across the Permian-Triassic boundary. *Palaeogeography, Palaeoclimatology, Palaeoecology* **231**, 315–321 (2006).
202. Maruoka, T., Koeberl, C., Hancox, P. J. & Reimold, W. U. Sulfur geochemistry across a terrestrial Permian-Triassic boundary section in the Karoo Basin, South Africa. *Earth and Planetary Science Letters* **206**, 101–117 (2003).
203. Grasby, S. E., Them, T. R., Chen, Z., Yin, R. & Ardakani, O. H. Mercury as a proxy for volcanic emissions in the geologic record. *Earth-Science Reviews* vol. 196 102880 (2019).
204. Dal Corso, J. *et al.* Permo–Triassic boundary carbon and mercury cycling linked to terrestrial ecosystem collapse. *Nature Communications* **11**, 2962 (2020).
205. Rugenstein, M. A. A., Sedláček, J. & Knutti, R. Nonlinearities in patterns of long-term ocean warming. *Geophysical Research Letters* **43**, 3380–3388 (2016).
206. Yang, H. & Zhu, J. Equilibrium thermal response timescale of global oceans. *Geophysical Research Letters* vol. 38 L14711 (2011).
207. Song, H. *et al.* Anoxia/high temperature double whammy during the Permian-Triassic marine crisis and its aftermath. *Scientific Reports* **4**, 4132 (2014).
208. Alroy, J. Accurate and precise estimates of origination and extinction rates. *Paleobiology* **40**, 374–397 (2014).
209. Scotese, C. R. Atlas of Permo-Triassic Paleogeographic Maps (Mollweide Projection), Maps 43 - 52, Volumes 3 & 4 of the PALEOMAP Atlas for ArcGIS, PALEOMAP Project, Evanston, IL. *Technicla Report* **3**, (2014).
210. Zhang, F. *et al.* Two distinct episodes of marine anoxia during the Permian-Triassic crisis evidenced by uranium isotopes in marine dolostones. *Geochimica et Cosmochimica Acta* **287**, 165–179 (2020).
211. Wu, Y. *et al.* Six-fold increase of atmospheric pCO2 during the Permian–Triassic mass extinction. *Nature Communications* **12**, 2137 (2021).
212. Grossman, E. L. & Joachimski, M. M. Oxygen Isotope Stratigraphy. in *Geologic Time Scale 2020* 279–307 (2020). doi:10.1016/b978-0-12-824360-2.00010-3.
213. Trotter, J. A., Williams, I. S., Barnes, C. R., Männik, P. & Simpson, A. New conodont δ18O records of Silurian climate change: Implications for environmental and biological events. *Palaeogeography, Palaeoclimatology, Palaeoecology* **443**, 34–48 (2016).
214. Kaiho, K. *et al.* End-Permian catastrophe by a bolide impact: Evidence of a gigantic release of sulfur from the mantle. *Geology* **29**, 815–818 (2001).
215. Chu, D. *et al.* Lilliput effect in freshwater ostracods during the Permian-Triassic extinction. *Palaeogeography, Palaeoclimatology, Palaeoecology* **435**, 38–52 (2015).
216. Shen, J. *et al.* Mercury evidence of intense volcanic effects on land during the permian-triassic transition. *Geology* **47**, 1117–1121 (2019).
217. Cao, C., Wang, W., Liu, L., Shen, S. & Summons, R. E. Two episodes of 13C-depletion in organic carbon in the latest Permian: Evidence from the terrestrial sequences in northern Xinjiang, China. *Earth and Planetary Science Letters* **270**, 251–257 (2008).

218. Shen, J. *et al.* Evidence for a prolonged Permian–Triassic extinction interval from global marine mercury records. *Nature Communications* **10**, 1563 (2019).
219. Wang, X. *et al.* Mercury anomalies across the end Permian mass extinction in South China from shallow and deep water depositional environments. *Earth and Planetary Science Letters* **496**, 159–167 (2018).
220. Holser, W. T. *et al.* A unique geochemical record at the Permian/Triassic boundary. *Nature* **337**, 39–44 (1989).
221. Korte, C. & Kozur, H. W. Carbon-isotope stratigraphy across the Permian-Triassic boundary: A review. *Journal of Asian Earth Sciences* **39**, 215–235 (2010).
222. Luo, G. *et al.* Stepwise and large-magnitude negative shift in δ13Ccarb preceded the main marine mass extinction of the Permian-Triassic crisis interval. *Palaeogeography, Palaeoclimatology, Palaeoecology* **299**, 70–82 (2011).
223. Shen, S. zhong *et al.* High-resolution δ13Ccarb chemostratigraphy from latest Guadalupian through earliest Triassic in South China and Iran. *Earth and Planetary Science Letters* **375**, 156–165 (2013).
224. Hermann, E. *et al.* A close-up view of the Permian-Triassic boundary based on expanded organic carbon isotope records from Norway (Trøndelag and Finnmark Platform). *Global and Planetary Change* **74**, 156–167 (2010).
225. Luo, G. *et al.* Vertical δ13Corg gradients record changes in planktonic microbial community composition during the end-Permian mass extinction. *Palaeogeography, Palaeoclimatology, Palaeoecology* **396**, 119–131 (2014).
226. Schneebeli-Hermann, E. *et al.* Evidence for atmospheric carbon injection during the end-permian extinction. *Geology* **41**, 579–582 (2013).
227. Williams, M. L., Jones, B. G. & Carr, P. F. The interplay between massive volcanism and the local environment: Geochemistry of the Late Permian mass extinction across the Sydney Basin, Australia. *Gondwana Research* **51**, 149–169 (2017).
228. Wu, Y. *et al.* Organic carbon isotopes in terrestrial Permian-Triassic boundary sections of North China: Implications for global carbon cycle perturbations. *Bulletin of the Geological Society of America* **132**, 1106–1118 (2020).
229. Grasby, S. E., Liu, X., Yin, R., Ernst, R. E. & Chen, Z. Toxic mercury pulses into late Permian terrestrial and marine environments. *Geology* **48**, 830–833 (2020).

ACKNOWLEDGEMENTS

We thank Sarah Greene (University of Birmingham) for useful discussion of Earth System modelling. We thank "Ecosystem resilience and recovery from the Permo-Triassic crisis" project (EcoPT; grant NE/P013724/1), which is a part of the Biosphere Evolution, Transitions and Resilience (BETR) Program. HS, DC and JDC acknowledge support from the National Natural Science Foundation of China (41821001, 42072025, 42172031). MMJ and YS acknowledge support from the German Science Foundation (Grant JO 219/16 within DFG Research Unit TERSANE/FOR 2332).

AUTHOR CONTRIBUTIONS

JDC coordinated the developing of the article. All authors contributed to the writing of the manuscript and building of the figures.

COMPETING INTERESTS

The authors declare no competing interests.

DATA AVAILABILITY STATEMENT

Data from the Paleobiology Database used for the new calculation of the marine extinction rate are available in the Supplementary Materials.

FIGURE CAPTIONS

Figure 1. The Permian–Triassic mass extinction and its world. The PTME, also know as the "Great Dying", is the largest extinction of the entire Phanerozoic, with severe losses both in marine and terrestrial ecosystems. The PTME world consisted of one single continent (Pangea) surrounded by a vast ocean (Panthalassa), and a giant gulf (Palaeo- and Neo-Thetys). The Siberian Traps Large Igneous Province erupted 2–7 million km^3 of basalt in the northern hemisphere during the PTME. The biological crisis was the result of the environmental changes triggered by the volcanic emissions from the Siberian Traps, including the gasses released by contact metamorphism caused by magmatic intrusions in the host rocks, such as CO_2, CH_4, SO_2, halogens and metals, into the Permian–Triassic atmosphere–ocean system. **a)** Newly calculated Gap-filler (GF) extinction rates [208] (Supplementary Note 1) for marine animals show the PTME stands out as the most severe extinction event compared to other intervals. Along with the PTME, the Ordovician–Silurian, Frasnian–Famennian, end-Triassic, end-Cretaceous mass extinctions are usually regarded as the largest extinction events of the Phanerozoic, also known as the "Big 5". **b)** Palaeogeographic reconstruction of Earth during the Permo–Triassic transition. Palaeogeography is from ref. [209]. GSSP = Global Stratotype Section and Point.

Figure 2. Marine mass extinction. Pattern of the extinction in marine settings and major recorded geochemical changes. High-resolution geochemical data coupled to species richness of different marine groups. Palaeontological data show two extinction pulses spanning the Permian–Triassic boundary (PTB). While the first pulse appears to be synchronous in different areas, the second major pulse of extinction may have been diachronous. Geochemical changes mark the marine extincion interval (the interval between the two pulses), and tastify for major environmental changes coeval to the biological crisis, as global warming ($\delta^{18}O$), oceanic anoxia (Uranium-isotope, $\delta^{238}U$, and sulfur-isotope of carbonate-associated sulphate, $\delta^{34}S_{CAS}$), and ocean acidification (Boron-isotope, $\delta^{11}B$, calcium-isotope, $\delta^{44/40}Ca$). Carbon-isotope ($\delta^{13}C$) data come from the most updated compilations of ref. [210,211]. Oxygen-isotope ($\delta^{18}O$) data from conodont apatite are from StabisoDB (Stable Isotope Database for Earth System Research) [212]. $\delta^{18}O$ data measured with SIMS (Secondary Ion Mass Spectrometer) have been corrected by a factor of -0.6‰ according to estimates by ref. [213] of the offset between conodont *in-situ* SIMS and bulk IRMS (Isotope Ratio Mass Spectrometer) analyses. Uranium-isotope ($\delta^{238}U$) data are from ref. [210]. $\delta^{34}S_{CAS}$ data are from ref. [173,179,214]. $\delta^{11}B$ data from brachiopod calcite are from ref. [182]. $\delta^{44/40}Ca$ data are from ref. [186]. Species richness from numerous PTB sections in South China is from ref. [4]. Genera richness from the Dolomites (Southern Alps, Italy) is from refs. [24,25].

Fig. 3. Extinction selectivity during the Permian–Triassic mass extinction. The pattern of the PTME suggests statistically significant extinction selectivity between different ecological groups, shedding lights on the causes of the marine mass extinction. However, even if selectivity clearly played a role, high extinction rates are recorded for all marine ecological groups. **a)** Summary of extiction selectivity trends observed in marine animals: Based on refs. [4,37,38,41–44,183,194]. **b)** Extinction magnitude among different ecological groups in South China [4]. There are significant differences (Mann Whitney test, $p<0.05$) between extinction severity among different ecologic groups, i.e., nekton *vs* benthos, buffered *vs* unbuffered, and bivalve *vs* brachiopod. Selectivity between motile and non-motile animals appears to have been less significant ($p=0.05$). Bars represent 95% confidence intervals. **c)** Ecological selectivity of global extinctions during the PTME [43]. A zero log-odds value means there is no association between the ecological traits and extinction. The unbuffered and carbonate-shell genera were preferentially killed ($p<0.05$). Selectivity between narrow-geographic- and cosmopolitan-range genera is weaker. Selectivity among genera with calcite shell, infaunal, and lower abundance of individuals is not significant ($p>0.05$).

Figure 4. Terrestrial mass extionction. Pattern of the extinction in terrestrial settings and major recorded geochemical changes. Organic C-isotope ($\delta^{13}C_{TOC}$), Hg and Hg/TOC, and main biological events from reference sections of the terrestrial PTME in Northwestern China [102,215–217], South China [27,71,82], Sydney Basin [26,67] and Karoo Basin [28,95], and correlation with the marine $\delta^{13}C_{carbonate}$ and $\delta^{13}C_{TOC}$ (Meishan only) records [217]. The $\delta^{13}C_{TOC}$ record from Meishan has been used as a chemostratigraphic tool to correlate the marine GSSP to the terrestrial sections of Northwestern China [217]. Data from the terrestrial PTME records with high-resolution chemostratigraphic data and/or redioisotopic ages, which allow correlation with the marine PTME, indicate that the terrestrial crisis started before the marine mass extinction. *Gigantopteris* and *Glossopteris* forests collapsed 60 kyrs (South China) [27,204] to 370 kyrs (Sydney Basin) [26,67] before the marine extinction. Wildfire activity widespreadly increased [27,67]. Tetrapods experienced high extinction rates, probably over a relatively long interval of up to ~1 Myr [95]. Existing data strongly support that the terrestrial crisis started before the global marine mass extincion. Evidence of also an earlier marine crisis come from high-latitude northwetern margin og Pangea.

Figure 5. Link between Siberian Traps, extinction, C-cycle changes and global warming. Radiomatric ages of the volcanic products (lava, tuff, and sills) of the Siberian Traps Large Igneous Province (STLIP) and sedimentary Hg geochemistry (BOX 2) indicate this LIP was active during the PTME, and was linked to injection of isotopically-light carbon into the Permian–Triassic atmosphere–ocean system, as inferred by the C-isotopes ($\delta^{13}C$) record (BOX 1), which rised pCO_2 and increased global temperature, as shown by O-isotopes ($\delta^{18}O$) of conodont apatite. Different volcanic phases can

be defined: a first mainly pyroclastic phase (lava and tuff), a second mainly intrusive phase (sills), and a final extrusive phase. **a)** Schematic map of the STLIP (adapted from refs. [119,129]) showing the predominance of lava, pyroclastic and subvolcanic magmatic products over cratonic and non-cratonic regions of this vast province. M-K stands for Maymecha-Kotuy. **b)** Geochemical data linking the STLIP to extinction and environmental changes. Dating U/Pb ages of intrusive and extrusive rocks of the Siberian Traps are from ref. [18,21]. Hg and Hg/TOC data are from ref. [218,219]. Only Hg/TOC data with TOC>0.2% have been plotted following the approach of ref. [203]. Source of $\delta^{13}C$ and $\delta^{18}O$ data as in Fig. 2. Time span of marine and terrestrial extinction intervals are as defined in Fig. 2. The eruption of STLIP was very likely the trigger of the Permian–Triassic mass extinction.

Figure 6. Extinction mechanisms. Summary of the volcanically-triggered extinction mechanisms inferred from the geochemical, sedimentary and palaeontological record of the PTME and their recorded effects on biota. The initial mainly extrusive–pyroclastic volcanic phase is coeval with the initial terrestrial crisis, whilst the onset of intrusive volcanism is coeval with the marine extinction interval. The different volcanic styles and linked injection of greenhouse gases, halogens and metals (only the most relevant volcanic/volcanogenic gases are represented in the figure) in the end Permian–earliest Triassic atmosphere–land–ocean system, triggered a cascade of environmental disturbances, which firstly affected terrestrial ecosystems and high-latitude marine environments, and then marine biota. The effects of the environemtal changes on the physiology and ecology of terrestrial and marine biota were multiple, showing that a fatal combination of factors, each having selective effects on biota, led to the most severe extinction of the Phanerozoic.

BOX 1: The Permian–Triassic boundary C-isotope record

Carbon isotopes ($\delta^{13}C$) are used as a chemostratigraphic tool to correlate marine and terrestrial successions around the world. Many high resolution $\delta^{13}C$ records have been collected across the PTB and they provide a powerful correlation tool, which helps identifying the PTME interval and link biological and environmental phenomena recorded in different locations. Major $\delta^{13}C$ shifts in carbonate ($\delta^{13}C_{carbonate}$) [220–223], and marine and terrestrial total organic carbon ($\delta^{13}C_{TOC}$) [221,224,225], are documented during the PTME (Figs. 2 and 3). A 3–6‰ negative $\delta^{13}C_{carbonate}$ excursion begins gradually in the lower C. yini Zone (*C. bachmanni* Zone) ~60 kyrs below the onset of the marine crisis [59,221], before accelerating to reach a minimum values in the earliest Triassic (*H. parvus* to early *I. isostichia* Zone). Similar shifts are recorded by $\delta^{13}C$ values from total organic matter, wood and leaves, allowing correlation of non-marine to marine records (for example refs. [217,225–228]; Fig. 2 and 3). However, because $\delta^{13}C_{TOC}$ is dependent on variable contributions of algal vs. bacterial and marine vs. terrigenous organic matter, some records display non-parallel trends in $\delta^{13}C_{carbonate}$ and $\delta^{13}C_{TOC}$, as documented, for example, at Meishan GSSP section [225]. A variety of mechanisms were suggested to explain the negative $\delta^{13}C$ shifts by the addition of isotopically light carbon to the exogenic carbon-cycle reservoirs. Besides soil erosion, reduced primary productivity and destabilization of gas hydrates, Siberian Traps volcanism and related processes were favoured as the ultimate cause. Identification of the source of the isotopically light carbon and its $\delta^{13}C$ signature is critical to estimate the amount of carbon transferred into the PTB atmosphere–ocean system, and to model atmospheric pCO_2 increase, temperature rise and seawater pH decline.

BOX 2: Tracing Siberian Traps activity in the sedimentary record

Significant increases in mercury (Hg) concentrations above background occur at marine and terrestrial PTME boundaries globally, and have been attributed to Hg emissions from the Siberian Traps Large Igneous Province (STLIP) [27,126,203]. If correct, Hg serves as a 'fingerprint' of STLIP in the sedimentary record, allowing temporal correlation between the eruption and the extinction with resolution on a millennial time scale [229]. As a volatile gas Hg has sufficient atmospheric residence time for inter-hemispheric mixing, until eventually being transferred through wet or dry deposition to the marine and terrestrial environment, and after going through various biogeochemical cycling, eventual geologic sequestration in sediments [203,229]. In theory then, enhanced Hg emissions related to the STLIP should be recorded as an Hg spike in sediments [229]. This is not definitive though as concurrent changes in sequestration pathways, such as enhanced bioproductivity and consequent increased organic matter drawdown, could also create Hg spikes. Careful analyses of Hg data and sequestration pathways is required before a linkage with STLIP is possible. Stable isotope data (Fig. 3), particularly mass independent fractionation (MIF), support Hg anomalies in offshore marine deposits being largely derived from a volcanic source [203]. However, these same data show nuances in the Hg cycle. Nearshore deposits have Hg spikes with a MIF signature of terrestrial vegetation [203], likely related to devastation of forest and swamp ecosystems at that time [203,204]. Whether Hg anomalies are directly from volcanos, or indirectly from terrestrial reservoirs released through STLIP induced global warming, they both serve as a fingerprint (or LIP mark) of STLIP. Resolving the relative Hg pathways requires further work, along with understanding of how terrestrial and marine Hg records can be used to resolve the apparent diachronous extinction. Figure is adapted from ref. [203]

GLOSSARY (in alphabetic order)

ALKALINE
Any rock of a magmatic series presenting a high content of alkali (Na_2O and K_2O) relative to silica (SiO_2).

BIOSTRATIGRAPHY
Technique to determine the relative age of sedimentary rocks using their fossil content.

CHEMOSTRATIGRAPHY
The study of geochemical variations in sedimentary rocks; Globally-recorded chemostratigraphic changes are used to correlate sedimentary sequences.

CONODONT
The hard part of an extinct jawless vertebrates, similar to an eel.

EVOLUTIONARY FAUNA
A fauna type that typically shows an increase in biodiversity following a logistic curve, i.e., Cambrian fauna, Paleozoic fauna, and Modern fauna.

FRAMBOIDAL PYRITE
Aggregates of pyrite (sulfide mineral, FeS_2) with a “ruspberry” (“la framboise” in french) aspect. It is used as a palaeo-redox proxy.

GSSP
Global Stratotype Section and Point. Reference stratigraphic section and level where boundaries between geological stages, for example between the Permian and the Triassic, are defined.

JUVENILE VOLATILE
A gas species that is dissolved in, or exsolved from, a magma, and is thus newly introduced to the atmosphere when the magma reaches the Earth´s surface.

LARGE IGNEOUS PROVINCE
Rapidly emplaced (<1–5 Myrs) volcanic provinces with areal extents >0.1 million km^2 and volumes >0.1 million km^3.

MASS EXTINCTION
Global biological events of greatly elevated extinction rates.

OCEANIC ANOXIC EVENT
Interval of severely reduced dissolved oxygen content in the ocean.

ORIGINATION RATES
The ratio of the number of newly occurring species/genera to the total number over a given geological period.

PYROCLASTIC
Volcanic rock composed by fragmented pieces of lava. Coarser pyroclastic fragments accumulate in proximity to the erupting vent, while finer particles can travel hundreds of kilometres.

PYROXENITIC MANTLE SOURCE
A mantle source dominated by the presence of pyroxene and by paucity or lack of olivine. They represent enriched and very fertile mantle lithologies.

RADIOISOTOPE DATING
Technique to determine the absolute age of rocks using radioactive decay.

SIGNOR-LIPPS EFFECT

A paleontological principle which states that the fossil record of organisms is never complete.

SILL
A tabular subvolcanic magma-body, emplaced roughly concordant or to the general bedding (stratification or layering) of its host-rocks.

SPORE TETRAD
Four connected immature spore grains in tetrahedral or tetragonal fashion produces by meiotic microsporogenesis.

TERATOLOGICAL SPOROMORPHS
Pollen and spores that present congenital abnormalities, such as lack of full development and malformations in their structure.

THOLEIITIC
Sub-alkaline series of magmatic rocks, which undergo iron enrichment during differentiation due to their poorly oxidised state. Tholeiites are the products of extensive melting of the mantle.

a

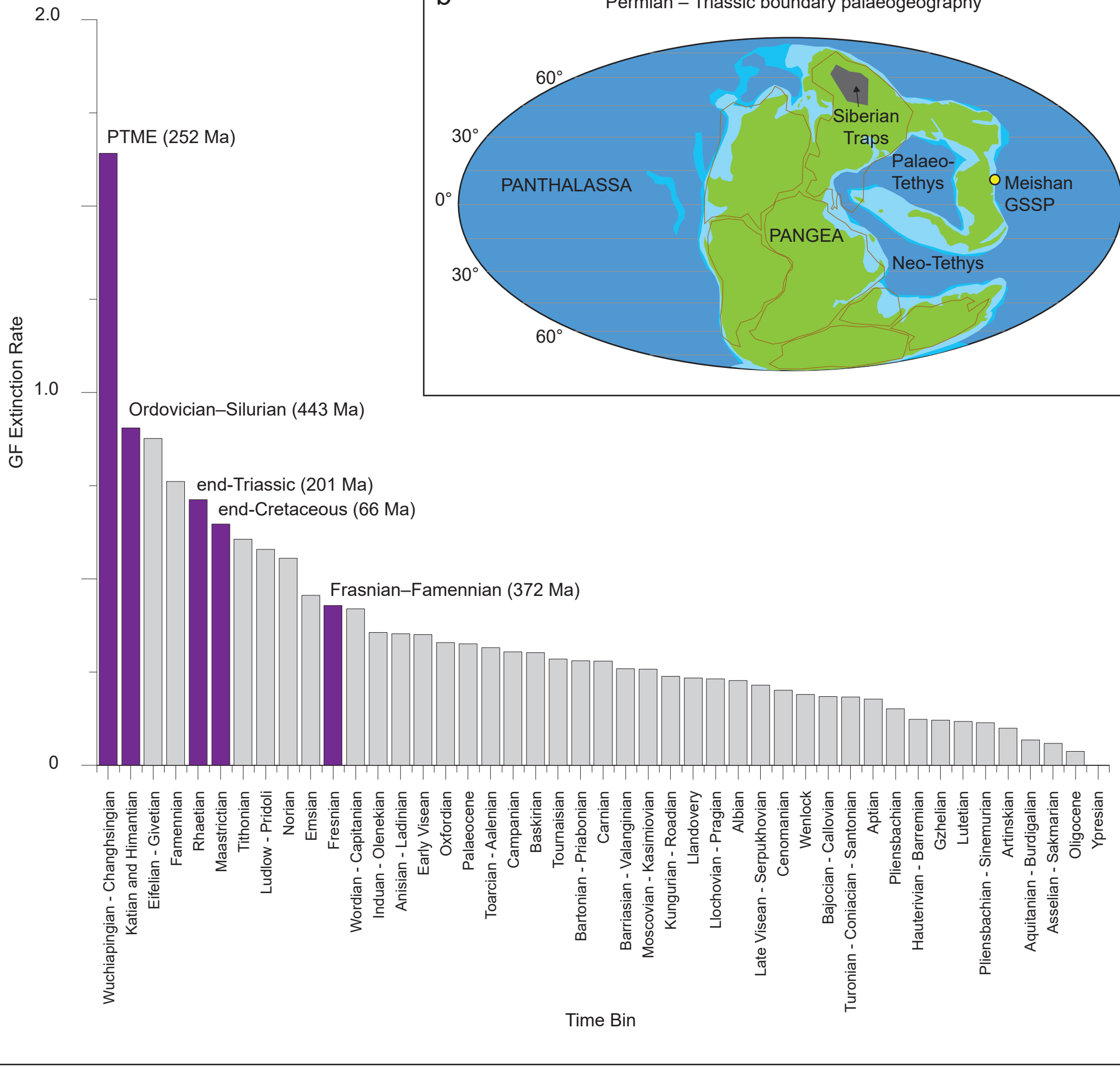
2.0
1.0
0
GF Extinction Rate
PTME (252 Ma)
Ordovician–Silurian (443 Ma)
end-Triassic (201 Ma)
end-Cretaceous (66 Ma)
Frasnian–Famennian (372 Ma)
Wuchiapingian - Changhsingian
Katian and Himantian
Eifelian - Givetian
Famennian
Rhaetian
Maastrictian
Tithonian
Ludlow - Pridoli
Norian
Emsian
Fresnian
Wordian - Capitanian
Induan - Olenekian
Anisian - Ladinian
Early Visean
Oxfordian
Palaeocene
Toarcian - Aalenian
Campanian
Baskirian
Tournaisian
Bartonian - Priabonian
Carnian
Barriasian - Valanginian
Moscovian - Kasimiovian
Kungurian - Roadian
Llandovery
Llochovian - Pragian
Albian
Late Visean - Serpukhovian
Cenomanian
Wenlock
Bajocian - Callovian
Turonian - Coniacian - Santonian
Aptian
Pliensbachian
Hauterivian - Barremian
Gzhelian
Lutetian
Pliensbachian - Sinemurian
Artinskian
Aquitanian - Burdigalian
Asselian - Sakmarian
Oligocene
Ypresian
Time Bin

b

Permian – Triassic boundary palaeogeography
60°
30°
0°
30°
60°
PANTHALASSA
Siberian
Traps
Palaeo-
Tethys
Meishan
GSSP
PANGEA
Neo-Tethys

PALAEONTOLOGICAL RECORD

Conodont biostratigraphy

TRIASSIC

I. isarcica

I. staeschei

PTB

H. parvus

PERMIAN

C. zhejiangensis

H. changxingensis

C. meishanensis

C. yini

251.80 — 251.85 — 251.90 — 251.95 — 252.00 Ma

ALL SPECIES

2nd pulse

1st pulse

Richness: 0 200 400

RUGOSE CORALS
FUSILINIDS
CALCAREOUS ALGAE
SPONGES
TRILOBITES
RADIOLARIANS
SMALL FORAMINIFERA
OSTRACODS
BRACHIOPODS
BIVALVES
GASTROPODS
AMMONOIDS
CONODONTS

Initial Number of Species: 4 13 13 3 2 21 102 41 85 47 27 25 30

ALL GENERA

2nd

1st

?

Richness: 0 50

ALGAE
FORAMINIFERA
BRACHIOPODS
MOLLUSCS
CONODONTS

Initial Number of Genera: 5 23 1 5 1

SOUTH CHINA — DOLOMITES, ITALY

GEOCHEMICAL RECORD

$\delta^{13}C_{carbonate}$ (‰ VPDB): -5 -3 -1 1 3 5

$\delta^{18}O_{apatite}$ (‰ VSMOW): 17 19 21

$\delta^{238}U$ (‰): -1 -0.2 0.6

$\delta^{34}S_{CAS}$ (‰ VCDT)

$\delta^{11}B_{brachiopod}$ (‰ NIST 951): 11 13 15

$\delta^{44/40}Ca_{apatite}$ (‰ SW): -0.9 -0.7

SIMS
IRMS

Meishan only

Meishan only

MARINE EXTINCTION INTERVAL

Geochemical proxy for

SEAWATER TEMPERATURE

SEAWATER REDOX CONDITIONS

OCEAN ACIDIFICATION

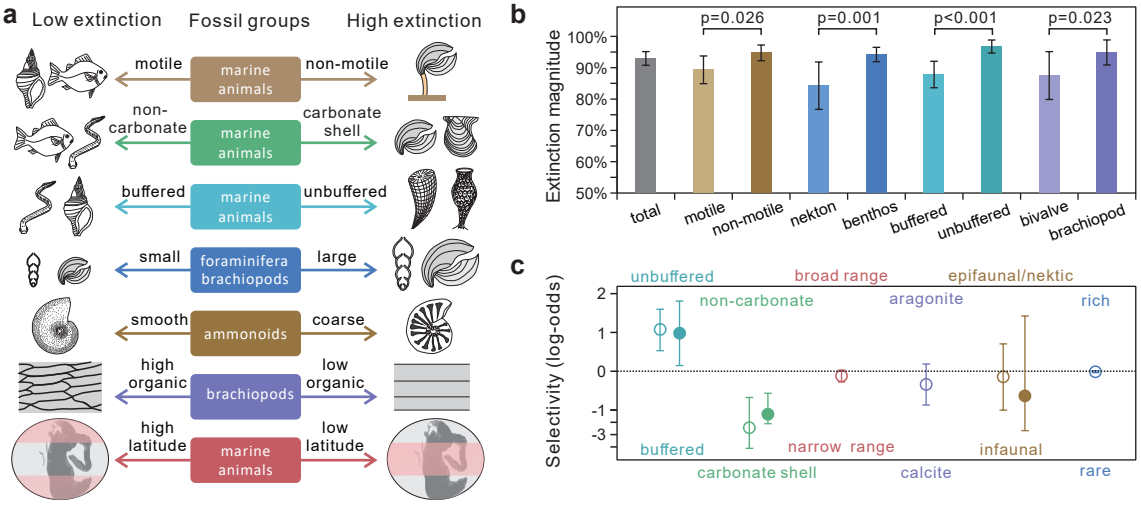
a
Low extinction
Fossil groups
High extinction
motile
marine animals
non-motile
non-carbonate
marine animals
carbonate shell
buffered
marine animals
unbuffered
small
foraminifera brachiopods
large
smooth
ammonoids
coarse
high organic
brachiopods
low organic
high latitude
marine animals
low latitude
b
Extinction magnitude
100%
90%
80%
70%
60%
50%
p=0.026
p=0.001
p<0.001
p=0.023
total
motile
non-motile
nekton
benthos
buffered
unbuffered
bivalve
brachiopod
c
Selectivity (log-odds)
2
1
0
-1
-3
unbuffered
broad range
epifaunal/nektic
non-carbonate
aragonite
rich
buffered
narrow range
infaunal
carbonate shell
calcite
rare

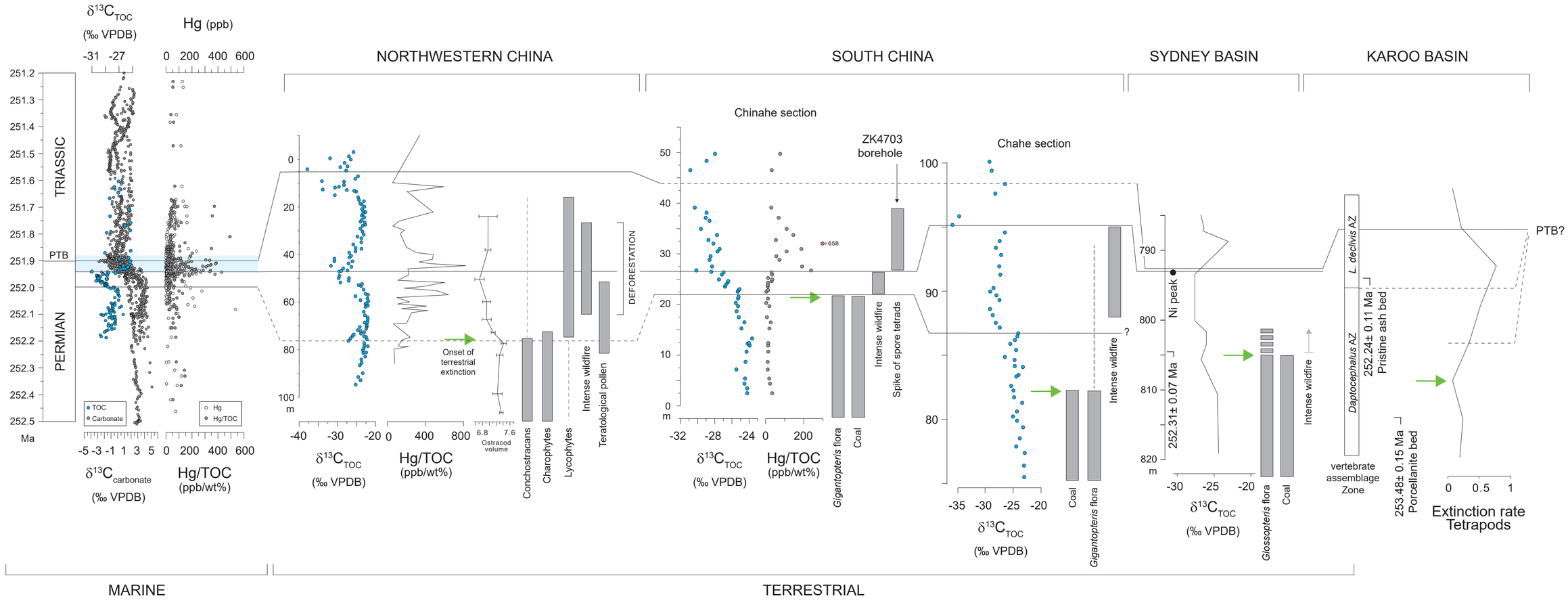
δ13CTOC (‰ VPDB)
Hg (ppb)
-31 -27
0 200 400 600
251.2
251.3
251.4
251.5
251.6
251.7
251.8
251.9
252.0
252.1
252.2
252.3
252.4
252.5
Ma
TRIASSIC
PERMIAN
PTB
TOC
Carbonate
Hg
Hg/TOC
-5 -3 -1 1 3 5
0 200 400 600
δ13Ccarbonate (‰ VPDB)
Hg/TOC (ppb/wt%)
MARINE
NORTHWESTERN CHINA
SOUTH CHINA
SYDNEY BASIN
KAROO BASIN
0
20
40
60
80
100
m
-40 -30 -20
0 400 800
δ13CTOC (‰ VPDB)
Hg/TOC (ppb/wt%)
Onset of terrestrial extinction
6.8 7.6
Ostracod volume
Conchostracans
Charophytes
Lycophytes
Intense wildfire
Teratological pollen
DEFORESTATION
Chinahe section
ZK4703 borehole
Chahe section
50
40
30
20
10
0
m
-32 -28 -24
0 200
δ13CTOC (‰ VPDB)
Hg/TOC (ppb/wt%)
658
Gigantopteris flora
Coal
Intense wildfire
Spike of spore tetrads
100
90
80
-35 -30 -25 -20
δ13CTOC (‰ VPDB)
Coal
Gigantopteris flora
Intense wildfire
?
790
800
810
820
m
Ni peak
252.31± 0.07 Ma
-30 -25 -20
δ13CTOC (‰ VPDB)
Glossopteris flora
Coal
Intense wildfire
L. declivis AZ
Daptocephalus AZ
252.24± 0.11 Ma
Pristine ash bed
vertebrate assemblage Zone
253.48± 0.15 Ma
Porcellanite bed
PTB?
0 0.5 1
Extinction rate
Tetrapods
TERRESTRIAL

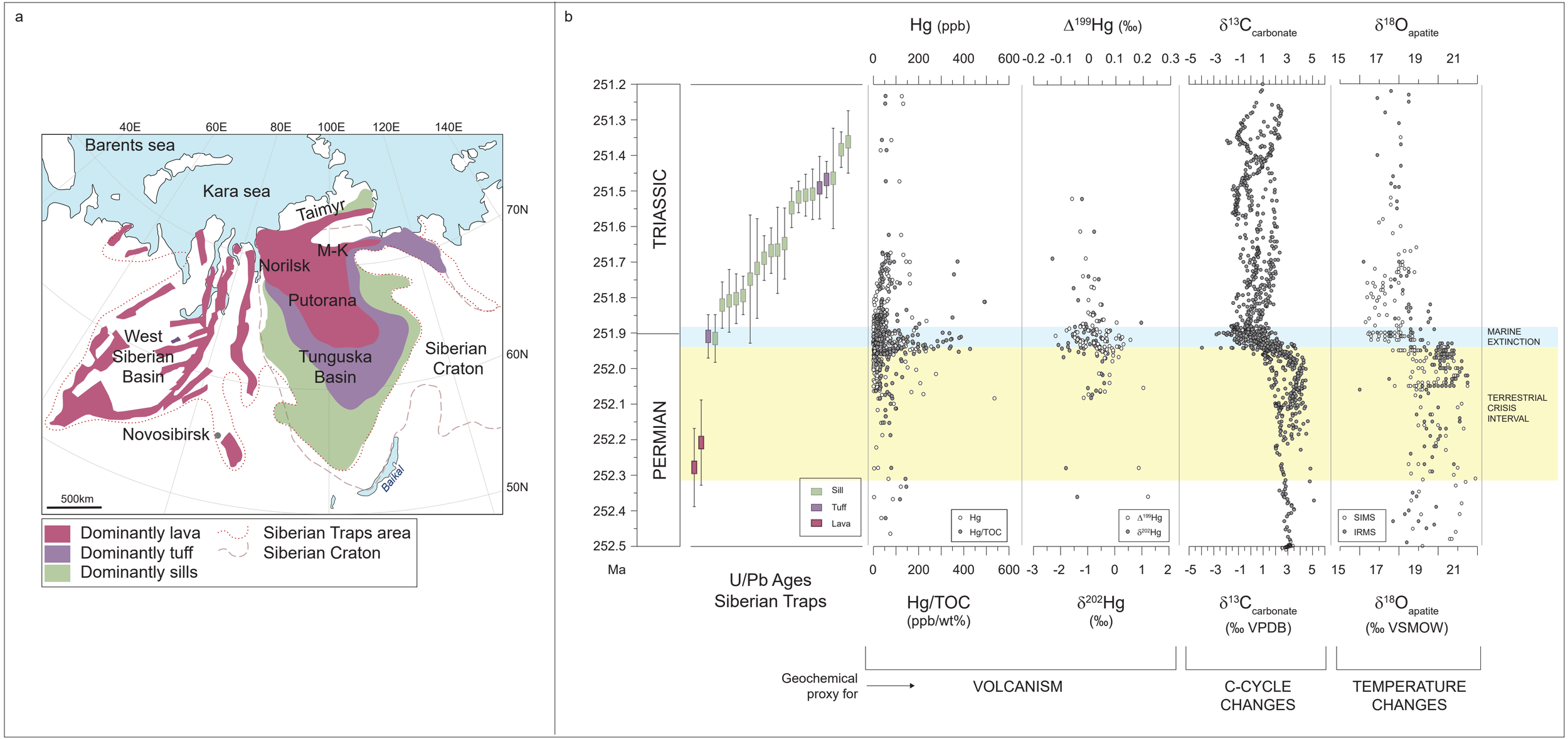
a
40E
60E
80E
100E
120E
140E
70N
60N
50N
Barents sea
Kara sea
Taimyr
M-K
Norilsk
Putorana
West
Siberian
Basin
Tunguska
Basin
Siberian
Craton
Novosibirsk
Baikal
500km
Dominantly lava
Dominantly tuff
Dominantly sills
Siberian Traps area
Siberian Craton
b
Hg (ppb)
Δ199Hg (‰)
δ13Ccarbonate
δ18Oapatite
0 200 400 600
-0.2 -0.1 0 0.1 0.2 0.3
-5 -3 -1 1 3 5
15 17 19 21
251.2
251.3
251.4
251.5
251.6
251.7
251.8
251.9
252.0
252.1
252.2
252.3
252.4
252.5
Ma
TRIASSIC
PERMIAN
MARINE
EXTINCTION
TERRESTRIAL
CRISIS
INTERVAL
Sill
Tuff
Lava
Hg
Hg/TOC
Δ199Hg
δ202Hg
SIMS
IRMS
0 200 400 600
-3 -2 -1 0 1 2
-5 -3 -1 1 3 5
15 17 19 21
U/Pb Ages
Siberian Traps
Hg/TOC
(ppb/wt%)
δ202Hg
(‰)
δ13Ccarbonate
(‰ VPDB)
δ18Oapatite
(‰ VSMOW)
Geochemical
proxy for
VOLCANISM
C-CYCLE
CHANGES
TEMPERATURE
CHANGES

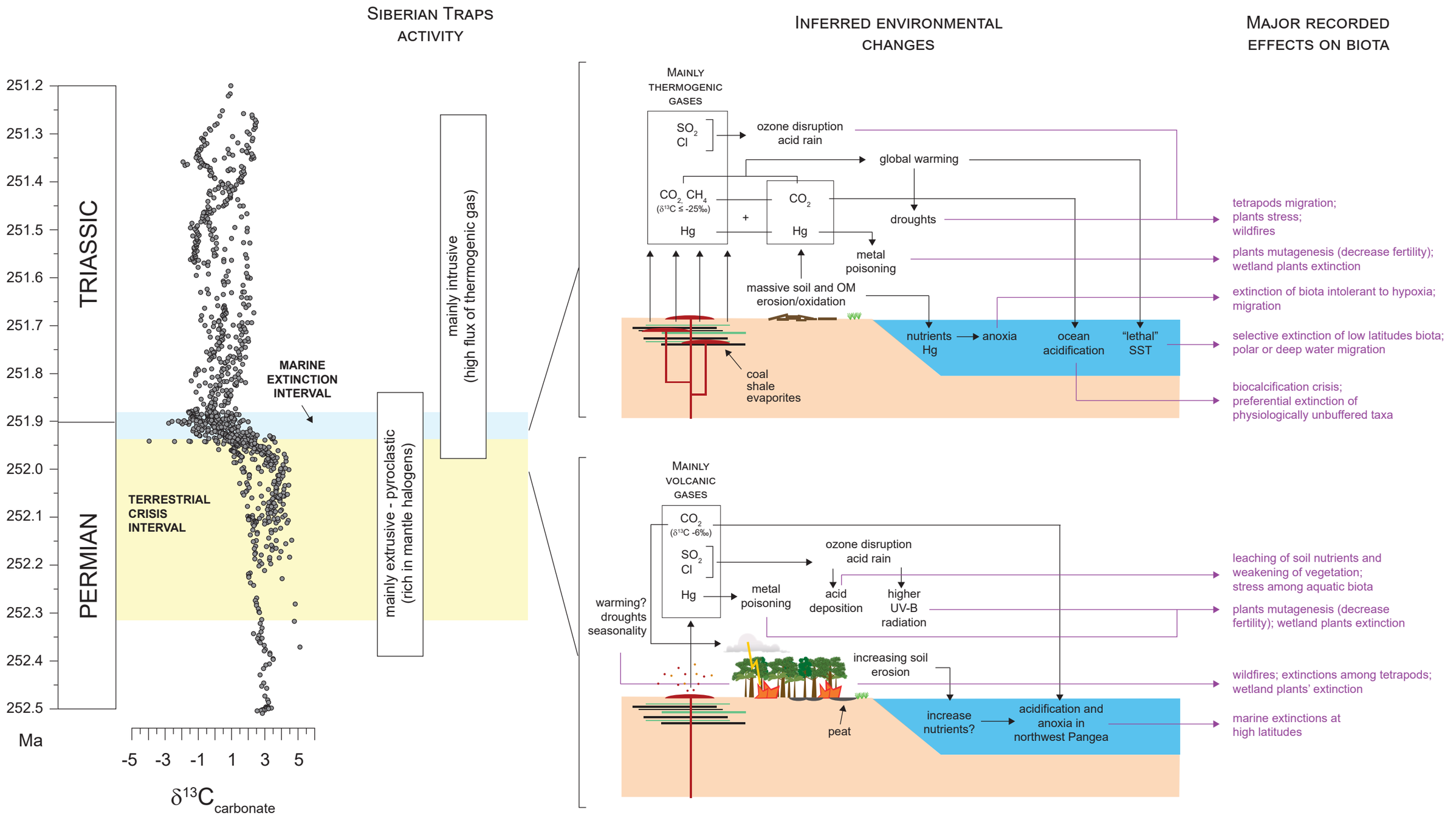
SIBERIAN TRAPS ACTIVITY
INFERRED ENVIRONMENTAL CHANGES
MAJOR RECORDED EFFECTS ON BIOTA
251.2
251.3
251.4
251.5
251.6
251.7
251.8
251.9
252.0
252.1
252.2
252.3
252.4
252.5
Ma
TRIASSIC
PERMIAN
MARINE EXTINCTION INTERVAL
TERRESTRIAL CRISIS INTERVAL
mainly intrusive (high flux of thermogenic gas)
mainly extrusive - pyroclastic (rich in mantle halogens)
-5 -3 -1 1 3 5
δ13Ccarbonate
MAINLY THERMOGENIC GASES
SO2 Cl
CO2, CH4 (δ13C ≤ -25‰)
Hg
+
CO2
Hg
ozone disruption acid rain
global warming
droughts
metal poisoning
massive soil and OM erosion/oxidation
nutrients Hg
anoxia
ocean acidification
"lethal" SST
coal shale evaporites
tetrapods migration; plants stress; wildfires
plants mutagenesis (decrease fertility); wetland plants extinction
extinction of biota intolerant to hypoxia; migration
selective extinction of low latitudes biota; polar or deep water migration
biocalcification crisis; preferential extinction of physiologically unbuffered taxa
MAINLY VOLCANIC GASES
CO2 (δ13C -6‰)
SO2 Cl
Hg
ozone disruption acid rain
metal poisoning
acid deposition
higher UV-B radiation
warming? droughts seasonality
increasing soil erosion
peat
increase nutrients?
acidification and anoxia in northwest Pangea
leaching of soil nutrients and weakening of vegetation; stress among aquatic biota
plants mutagenesis (decrease fertility); wetland plants extinction
wildfires; extinctions among tetrapods; wetland plants' extinction
marine extinctions at high latitudes

MERCURY CYCLING DURING THE SIBERIAN TRAPS EMPLACEMENT